

Tip-enhanced Raman imaging and spectroscopy: sensitivity, symmetry and selection rules

Catalin C. Neacsu, Samuel Berweger, and Markus B. Raschke

University of Washington, Department of Chemistry, Seattle, Washington, 98195-1700

This article reviews the new developments in Tip-enhanced Raman scattering (TERS). The fundamental mechanisms underlying the Raman enhancement are discussed, including the role of the plasmonic character of the metallic tips, the nature of the optical tip-sample coupling and the resulting local-field confinement responsible for ultrahigh spatial resolution down to just several nanometers. Criteria for the distinction of near-field signature from far-field imaging artifacts are addressed and TERS results of molecules and nanostructures are presented. With enhancement factors as high as 10^9 , single molecule spectroscopy is demonstrated. Spatially resolved vibrational mapping of crystalline nanostructures and determination of crystallographic orientation and domains is shown making use of the unique symmetry properties of the tip in conjunction with the intrinsic Raman selection rules.

1. Introduction

Optical spectroscopy provides nondestructive techniques for obtaining both structural and real time dynamic information of molecules and solids. Vibrational spectroscopy in particular, by directly coupling to the nuclear motion, offers insight into chemical composition, molecular bonds and their relative orientation, intermolecular coupling and zone-center phonons in crystalline solids [1, 2]. In that respect IR and Raman spectroscopy provide complementary information, with the feature of Raman spectroscopy of fewer constraints in terms of selection rules, readily providing access to low frequencies vibrations [3, 4, 5, 6], and being carried out in the vis-near IR spectral range in a comparably simple experimental design. However, with scattering cross-sections of $\sim 10^{-27}$ - 10^{-30} cm², the Raman response is weak, generally requiring probing a large molecular ensemble or bulk solids [7, 8].

It is highly desirable to combine the intrinsic chemical specificity of Raman spectroscopy with optical microscopy for the investigation of the spatial heterogeneity and composition of the analyte. In that regard the optical far-field Raman microscope has become an established tool for material characterization on the micrometer scale and in a confocal implementation with spatial resolution down to just several hundred nanometers [9]. However, for most applications the desired spatial resolution needed often exceeds the resolution imposed by far-field diffraction [10, 11].

Near-field Optical Microscopy (SNOM) provides access to higher spatial resolution [12, 13, 14, 15, 16, 17, 18, 19] and the aperture-based SNOM using tapered glass fiber tips has been employed for nano-Raman spectroscopy [20, 21, 22, 23]. However, the low optical throughput of the aperture probes (10^{-3} - 10^{-5}) severely limits the spatial resolution and the sensitivity that can be obtained, resulting in a long imaging time and parasitic Raman signal from the glass tip that could be an impediment [22].

High sensitivity in Raman scattering, in general, can be achieved by Surface-enhanced Raman spectroscopy (SERS) providing a strongly enhanced Raman response from molecular adsorbates on rough metallic surfaces or colloidal aggregates [24, 25, 26]. SERS is due to the near-field enhancement of the electromagnetic field at single or coupled metal nanostructures, often resonantly excited at their surface plasmon po-

lariton (SPP) eigenmodes [27, 28, 29, 30, 31, 32, 33, 34]. Together with a corresponding but weaker ($\sim 10^1$ - 10^2) chemical contribution [35] originating from surface bonding or charge transfer, the electromagnetic enhancement leads to a total increase in Raman signal by up to 14 orders of magnitude, allowing for detection down to the single molecule level [36, 37, 38, 39, 40, 41]. Despite its potential for chemically specific detection of minute amounts of analytes, it has remained challenging to develop SERS into a routine analytic spectroscopic tool, mostly due to difficulties associated with the reproducible fabrication of SERS-active substrates [42, 43, 44, 45].

In general, better control over the SERS active sites and their field enhancement can be achieved by what may be viewed as resorting to an inverse geometry with respect to SERS: suspension of the metal nanostructure providing the field enhancement at a small distance above the analyte [46]. This is the basis of tip-enhanced Raman scattering (TERS) making use of a single plasmon-resonant metallic nanostructure provided in the form of a scanning probe tip of suitable material and geometry.

Fundamentally, TERS is a variant of apertureless near-field optical microscopy (*s*-SNOM) [47, 48, 49, 50, 51]. All-optical resolution down to just several nanometers is provided by *s*-SNOM, in the visible [52, 53, 54] and IR spectral regions [55, 56, 57, 58]. TERS is the extension of this technique to inelastic light scattering, with the metallic tip used as active probe which provides both the local-field enhancement and serves as efficient scatterer for the Raman emission.

s-SNOM and special aspects of TERS have been addressed in recent reviews [18, 19, 59, 60, 61, 62] (and references therein), but no comprehensive discussion of the underlying physical mechanisms has yet been provided. Here, we review our recent progress in TERS and contribution to the understanding of near-field Raman enhancement and sensitivity, the tip-sample coupling, the spatial resolution, and we underline the importance of the plasmonic character of the tip and tip fabrication. In addition, we show that the unique symmetry properties of the tip-scattering geometry in combination with the Raman selection rules allows for the determination of crystallographic information on the nanoscale. This, together with the results of other groups, shows the potential of TERS

as a nano-analytical tool with diverse applications in material and surface science, and analytical chemistry for the study of biomolecular interfaces, molecular adsorbates, nanostructures and nanocomposites.

2. Tip-enhanced Raman spectroscopy (TERS)

TERS combines the advantages of SERS with those offered by *s*-SNOM: the single nanoscopic tip apex provides the local field enhancement at a desired sample location without requiring any special sample preparation [63, 64]. With the spatial resolution limited only by the tip apex size, chemical analysis on the nanometer scale is made possible. By raster scanning the sample, spatially resolved spectral Raman maps with nanometer resolution can be obtained simultaneously with the topography in atomic force microscopy (AFM) or surface electronic properties in scanning tunneling microscopy (STM).

The origin of the field enhancement at the tip apex is attributed to the singular behavior of the electromagnetic field (akin to the lightning-rod effect). In addition, the spatial confinement allows for the possible excitation of localized surface plasmon polaritons (tip-plasmons) for certain tip materials [65]. With the first effect being geometrical in origin, its magnitude is mainly dependent on the curvature of the apex. Taking advantage of the excitation of tip-plasmons can increase the overall enhancement by several orders of magnitude as will be discussed below.

Ultra-high sensitivity and nanometer spatial resolution imaging using TERS were obtained on various materials and molecular systems adsorbed on both flat and corrugated surfaces [66, 67, 68, 69, 70, 71, 72, 73, 74, 75, 76, 77, 78, 79, 80, 81, 82, 83, 84, 85]. Having large Raman cross-sections, several dye molecules (*e.g.*, malachite green, rhodamine 6G, brilliant cresyl blue) were used and near-field Raman enhancement factors up to $\sim 10^9$ were achieved [68, 71, 77, 81, 82]. Using Ag coated AFM tips, spatial resolution below 50 nm was obtained on surface layers of Rhodamine 6G dye molecules [68, 71]. Lateral resolution as high as 14 nm and a maximum Raman enhancement factor estimated at $\sim 10^4$ were obtained in spatially resolved probing vibrational modes along individual carbon nanotubes [72, 73, 78].

In studies of adenine as well as C_{60} molecules, the tip-induced mechanical force was shown to lead to mechanical strain induced frequency shifts of the normal Raman modes [74, 80]. Furthermore, it was observed that when interacting with individual metal atoms of the tip apex, adenine molecules form different isomers, demonstrating the potential TERS for atomic site selective sensitivity [83].

Extension of TERS implementation for coherent spectroscopy was shown for Coherent Anti-Stokes Raman scattering (CARS) of adenine molecules included in a DNA network [75]. Owing to the third order nonlinearity of the CARS process, the induced polarization at the tip apex is further confined, and higher lateral resolution is in principle possible [76].

Concomitant, theoretical studies on TERS report field en-

hancements up to three orders of magnitude in particular frequency regions [86, 87, 88, 89, 90, 91]. However, the expected resulting TERS enhancement of 12 orders of magnitude has not yet been observed experimentally.

In recent work from our group, we have refined the metallic tip fabrication, and experimentally identified and theoretically discussed the importance of the plasmonic properties of the scanning tip for achieving high Raman sensitivity [92, 93, 94, 95]. This has enabled near-field Raman enhancement factors of up to 10^9 from malachite green molecules adsorbed on smooth Au surfaces to be obtained, allowing for the detection of TERS response with single molecule sensitivity [81, 96].

The review is organized as follows: The experimental arrangement is presented in section 3. This includes the laser excitation and Raman detection, the metallic tip fabrication by electrochemical etching and the molecular systems used. Section 4 discusses the experimental characterization of the optical properties of the tips including their plasmonic behavior and the local-field enhancement factor as determined by second harmonic generation. Section 5 describes the theoretical analysis of the near-field distribution at the tip apex together with its spectral characteristics. The tip-sample optical coupling is discussed in section 6, where its effect on sensitivity, spatial resolution and spectral shift of the plasmon resonance are derived. The near-field character vs. far-field imaging artifacts in TERS and its polarization dependence are addressed in section 7. The procedure for estimating the near-field enhancement factor will be detailed and representative values are discussed. Tip-enhanced near-field spectra of monolayer and sub-monolayer of molecular adsorbates on smooth Au surface are given in section 8. The high sensitivity obtained and the dependency of the spectral features on the enhancement level is discussed. In section 9 we also address the important question of molecular bleaching and possible chemical contamination paths and show a number of control experiments. Near-field tip-enhanced Raman results with single molecule sensitivity are shown in section 10. This is concluded from the ultra-low molecular coverage and the observed intensity and spectral temporal fluctuations. We identify and propose in section 11 a new and promising extension of TERS for determination of both chemical and structural properties of nanocrystals. Section 12 gives an outlook on TERS, and novel ways to circumvent current instrumental difficulties are discussed.

3. Experimental

Various experimental schemes have been employed for TERS experiments. A tip axial illumination and detection geometry has been used, allowing for high NA, but requiring transparent samples or substrates [73, 97]. Similarly, but allowing to probe non-transparent samples, a high-NA parabolic mirror can be used [98, 99]. In both schemes, the tip is illuminated along the axial direction, with the tip apex positioned in the laser focus. For these geometries, polarization conditions require either a Hermite-Gaussian beam [100] or radial incident

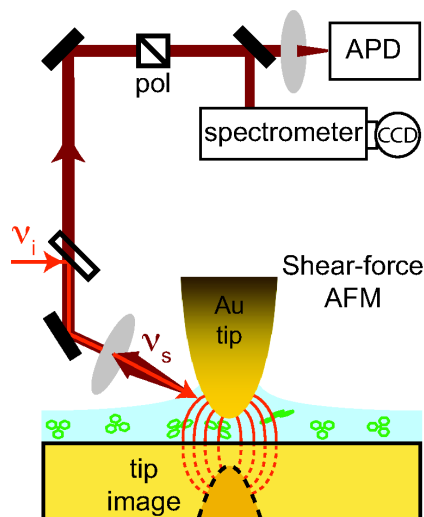


Figure 1: Schematic of the experimental TERS arrangement. The incident light is focused onto the tip-sample gap. The tip-backscattered and -enhanced Raman response is spectrally filtered using a notch filter and is spectrally resolved by an imaging spectrometer with N_2 (l) - cooled CCD or integrally detected by means of an avalanche photodiode (APD). Polarization directions of both incident and scattered light beams can be controlled independently. The blue layer indicates a thin surface water layer on the sample.

polarization [98, 101]. While allowing for efficient excitation and detection with the tip, independent polarization and k-vector control is limited, but desirable for symmetry selective Raman probing.

In contrast, side-on illumination and detection allows for greater flexibility in the selection of polarization and k-vector as well as the use of transparent samples. The scanning and tip-sample distance are controlled using either AFM or STM, with STM restricted to the use of conducting samples.

Fig. 1 shows the experimental layout of our side-illuminated TERS experimental arrangement. The incident radiation (v_i) is focused onto the tip-sample gap and the tip-scattered Raman light (v_s) is detected. For the experiments described here, a shear-force AFM is used. Unlike dynamic non-contact AFM, shear-force AFM maintains a constant height of several nm above the sample. Due to the short range tip-sample distance dependence of the field enhancement, dynamic non-contact AFM is less suitable. The time-averaged signal is greatly reduced due to the oscillating tip action. Contact AFM, maintaining constant and small tip-sample distance, experiences strong forces, making it unfavorable for probing molecular or soft matter samples. In contrast, with the spatial range of shear-forces confined to within 25nm [102], the shear-force AFM tip is controlled in close proximity to the sample without actual physical contact.

The control mechanism in shear-force AFM is based on the near surface vibrational damping of a probe tip oscillating parallel to the surface. The nature of the shear-force damping mechanism is not yet fully understood [19], with a variety of mechanisms being discussed [103, 104, 105, 106]. It has been

suggested [107, 108] that the tip experiences viscous damping from a thin water layer adsorbed on the surface of the sample under ambient conditions [108, 109, 110]. This water layer, present on most hydrophilic samples, may play an important role in the surface diffusion of the analyte molecules and possibly transition of molecules to adsorb onto the tip.

As incident light source, a continuous wave Helium-Neon laser, with $\lambda_i = 632.8\text{nm}$ (1.92eV) is commonly used [2]. In our experiments, after passing through a laser-line filter, the light is focused onto the tip-sample gap by means of a long working distance microscope objective (NA = 0.35). The tip-backscattered light is collected with the same objective and spectrally filtered using a notch filter and the signal is detected using either an avalanche photodiode or spectrally resolved using a fiber-coupled imaging spectrograph with a N_2 (l)-cooled CCD detector. Even for large enhancements the signal intensities are weak and detector noise is one limiting factor. We therefore limit the spectral resolution to 25 cm^{-1} for the tip-enhanced experiments. Far-field spectroscopic studies of molecular monolayers serving as reference to quantify the enhancement are conducted using a micro-Raman confocal setup, based on an inverted microscope (Zeiss Axiovert 135).

For our experiments we chose malachite green (MG), an organic triphenylmethane laser dye with an absorption peak around $\lambda \approx 635\text{ nm}$. The absorption peak of MG is very close to the laser energy used, leading to a resonant Raman excitation via the S_0 - S_1 electronic transition of the conjugated π -electron system, as discussed below [111]. To limit the rate of the molecular decomposition, the maximum fluence in the focus of the microscope objective was $5 \times 10^3 - 3 \times 10^4\text{ W/cm}^2$. However, molecular bleaching prevails under ambient conditions under resonant Raman excitation in TERS [81, 112].

Tip fabrication

The metallic scanning probe tips hold the central function in TERS studies providing the enhanced electromagnetic field at their apex. Ideally, as discussed below, they present strong plasmon resonances in the spectral region of interest, leading to enhanced pump (v_i) and scattered Raman fields (v_s) at the apex. Since the first experiments, the fabrication of suitable tips has been a major challenge, and a variety of methods for their fabrication have been used: angle-cutting the metal wire [113], DC or AC voltage electrochemical and milling procedures [114, 115, 116, 117], focused ion beam milling [54], metal-coating commercially available cantilever AFM tips [118, 119] and attaching spherical or other plasmonic nanoparticles to a glass tip [120]. Electrochemical etching [98, 121] is most commonly used due to perceived advantages [122] of tips fabricated in this manner.

For our experiments, we employ a DC voltage electrochemical etching method for both Au and W tips. It involves the anodic oxidation of the metal wire [123]. In the case of Au it involves the formation of soluble AuCl_4^- which subsequently

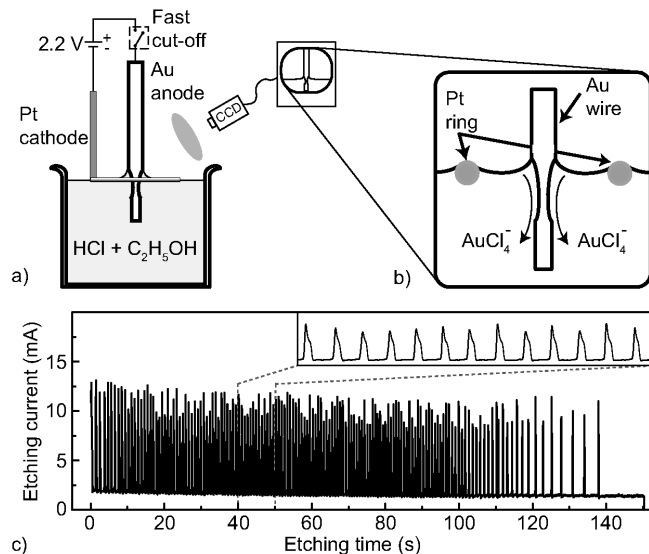


Figure 2: Schematics of the electrochemical etching cell. a) The Au wire (anode) is immersed partially into the solution. It is surrounded by the Pt cathode-ring. The evolution of the process is closely followed using a video microscope. b) The etching takes place just underneath the meniscus formed around the Au-wire. The flowing of AuCl_4^- is shown. For W-tips a similar procedure is used (see text). c) Time evolution of the etching current for a of 2.2 V. The current oscillation are periodic for about 100 seconds after which they become less frequent, although maintaining the amplitude. For periodic current oscillations (inset) tips with smooth surface and consistent taper are obtained.

diffuses away from the electrode [121]. The schematic of the electrochemical cell used is depicted in Fig. 2 panel a). After careful cleaning with acetone the Au wire ($\phi=0.125$ mm, purity 99.99%, temper as drawn, Advent Research Materials Ltd.) is partially immersed (~ 2 -3 mm) into the electrolyte solution. As electrolyte a 1:1 mixture of hydrochloric acid (HCl, aq. 37%) and ethanol is used. As the cathode, a platinum wire ($\phi = 0.3$ mm) circular ring electrode with a diameter of ~ 1 cm is used. It is held at the surface of the electrolyte with the Au wire positioned at the center of the Pt ring. For the etching a potential of +2.2V is applied to the Au anode with respect to the Pt cathode. This voltage was determined by us as well as others [124] to produce the best tips. This value is well above the Au oxidation potential due in part to the activation energy along the reaction pathway [114].

When placed in the electrolyte solution, the surface tension causes a concave meniscus to form around the wire, as shown schematically in Fig. 2 panel b). The overall shape and aspect ratio of the tip after etching are primarily determined by the shape of the meniscus [121]. During etching a downward flow of AuCl_4^- along the wire can be observed. The resulting ion concentration gradient partially inhibits etching of the lower portion of the wire, resulting in a necking of the wire near the meniscus [125]. This proceeds until the lower section of the

wire falls off. The remaining upper part of the wire is then used as the TERS/AFM tip.

Since the tip remains in the solution under the meniscus after the detachment of the lower part, the circuit has to switch off as rapidly as possible, for further etching would result in blunt tips. A comparator breaks the etching voltage when the current value becomes smaller than an adjustable reference value determined from the current change associated with the drop of the lower tip.

Monitoring the etching current reveals periodic oscillations of the current, as is shown in Fig 2 c). For the potential of 2.2V, the etching will generally reach completion in approximately 150 seconds with an average baseline current of ~ 2 mA. After a short time of initial fluctuations, the period equilibrates and remains constant for the first ~ 100 seconds of the etching process. Towards the end of the etching process, the oscillation period continuously decreases until completion of the process.

These current oscillations have been attributed to the depletion of Cl^- near the surface of the electrode [121]. Initially the Au will react rapidly to form AuCl_4^- , depleting the Cl^- near the electrode-electrolyte interface, resulting in a period of high current. With decreasing local Cl^- concentration, the Au will more readily form an electrode-passivating layer of $\text{Au}(\text{OH})_3$ [126], leading to extended periods of decreased current. Upon restoring the Cl^- concentration, the passivating layer dissolves and another current spike occurs [127]. Associated with the complex nature of the details of this oscillating electrochemical process, it is sensitively dependent on the applied potential. An empirically established etching voltage leads to the most periodic oscillations and results in the highest quality tips.

It is desirable to have a criterion to select suitable TERS tips other than scanning electron microscopy (SEM), which is known to deposit Raman - visible carbon contamination onto the tips due to electron-beam induced decomposition of trace organics in the residual gas [128, 129]. Tips etched under a constant oscillation period exhibit a smooth surface and consistent taper. In contrast, tips etched under conditions resulting in an inconsistent periodicity of the etching current frequently present deformities and large surface irregularities. We could verify in our experiments, by comparison of TERS activity with SEM of tip shape as well as the study of SPP of the tip apex, a link between homogeneous and smooth taper with TERS performance. Our observations here are in good agreement with previous work by Wang et. al [124].

A similar etching procedure is used for the tungsten tips. A W wire ($\phi = 200\mu\text{m}$) is partially immersed (~ 2 -3 mm) in aqueous 2 M KOH. A DC voltage of 3 V is applied between the wire and a stainless steel ring cathode.

Using these procedures tips with apex radii as small as 10nm are obtained. After etching, the tips are cleaned in distilled water and stored in isopropanol prior to usage, to avoid possible contamination in an otherwise uncontrolled atmosphere.

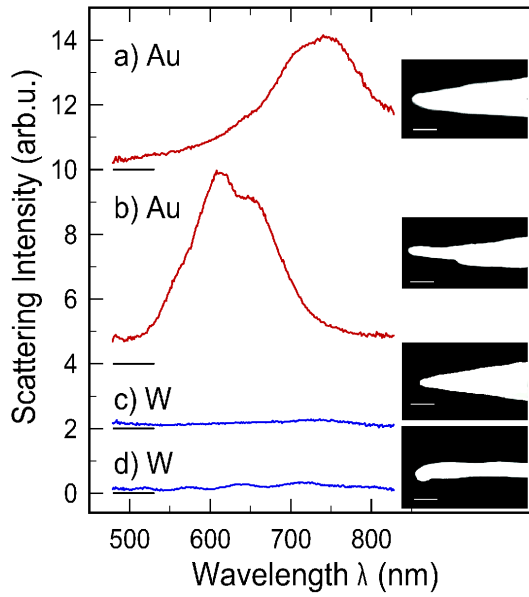


Figure 3: Scattering spectra for different Au and W tips. A plasmon-resonant behavior is observed for Au tips (a, b). Weaker and in general spectrally flat signal is observed in the case of W tips (c, d). The spectral data are juxtaposed with the electron microscope image from the corresponding tip. The scale bar corresponds to 100 nm [93].

4. Metallic tip optical characterization

Efficient local-field enhancement and TERS activity is in general associated with the excitation of local modes of surface plasmon polaritons (SPP) at the metallic tip [63, 73, 130, 131, 132]. However, determining the details of this correlation has remained an open problem. In the following we present the investigation of the spectral characteristics of the elastic light scattering from individual sharp metal tips and discuss the results in the context of the local plasmonic resonant behavior.

Surface plasmon polaritons of Au tips

Dark-field scattering spectroscopy with white light illumination would lead to a largely unspecific response with the scattering dominated by the tip shaft [133]. The SPP characteristics of the apex itself would become difficult to distinguish. Therefore, for the plasmonic light tip-scattering experiments we spatially limit the optical excitation to the near-apex region by use of evanescent wave excitation. For that purpose, the tip frustrates the evanescent field formed by total internal reflection on a prism base [134, 135] and the tip-scattered light is detected and spectrally analyzed. This confines the excitation to just several 100 nm from the tip apex. The complete description of the setup and the results is given elsewhere [93].

Fig. 3 shows representative scattering spectra for different Au (a, b) and W (c, d) tips. Both the excitation and detected light fields are unpolarized. All spectra are acquired for the tips within few nanometers above the prism surface, as controlled by shear-force AFM. The intensity scale is the same for all four cases, and the spectra are offset for clarity. Elec-

tron micrographs for the tip structures investigated are shown as insets.

The pronounced wavelength dependence of the scattering of Au tips is characteristic of a plasmon resonant behavior. Both scattering intensity and spectral position of the resonance are found to be sensitive with respect to structural details of the tips. In general, for regular tip shapes the resonance is characterized by one (Fig. 3 a) distinct spectral feature. Inhomogeneities in the geometric shape are reflected in spectral broadening and/or occurrence of multiple spectral features (Fig. 3 b). In addition, the spectral position and shape of the plasmon resonance depend sensitively on the aspect ratio of the tip.

For comparison, spectral light scattering by tungsten tips of similar dimensions is shown in Fig. 3 c and d. Overall weaker emission intensities are observed compared to Au tips. For W, a metal with strong polarization damping due to absorptive loss in the visible and near-IR region, no SPP resonance is expected. Here, a spectrally flat optical response is observed with weak overall scattering intensities (Fig. 3 c). The spectral behavior is found to show little variation with tip radius and tip cone angle, except for the case of very slender tips where a modulation is observed, as shown in Fig. 3 d).

A spectrally resolved tip-prism distance dependence measurement of the scattering intensity for a Au tip with apex radius of $r \sim 15$ nm is shown in Fig. 4 with the plasmonic resonance peak centered around $\lambda = 692$ nm. The scattered signal is normalized with respect to the evanescent source spectrum that varies as a function of distance [136]. An increase in scattered intensity with decreasing the tip-prism distance is seen as the tip frustrates rising evanescent field intensities. The absence of a change in the spectral scattering characteristics demonstrates that the signal intensity observed at the strong resonance is dominated by the tip-apex region, with the shaft contributing to a spectrally unspecific background.

From polarization dependent studies of the tip scattering process we have found that, in general, more intense scattering is observed for emission polarized parallel with respect to the tip axis (p -polarized emission), corresponding to the excitation of longitudinal plasmonic modes. The intensity ratio of p to s (emission orthogonal to the tip axis) is typically found to range between 2 to 5 with a maximum value of ~ 10 . In the context of the TERS experiments it must be noted that the s -polarized field is not expected to get enhanced near a surface. In this case, the optical polarization of the tip and the corresponding image polarization induced in the sample are oriented antiparallel, as discussed below.

Local-field enhancement from bare tips

The highly resonant characteristics observed for Au tips suggest strong local-field enhancements in the vicinity of the apex. The quantification of the near-field enhancement factor is a difficult task in general. Without an absolute reference, the enhancement factor cannot be quantified from these linear optical experiments. We therefore make use of the symmetry selectivity of the second order nonlinear optical response in

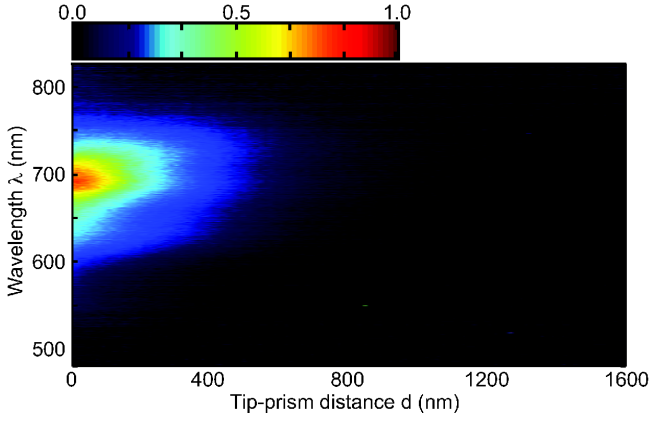


Figure 4: Spectrally resolved elastic scattering response of a Au tip approaching the evanescent white light generated at a prism base. A surface plasmon resonance centered around $\lambda = 690$ nm is observed. The absence of a spectral shift associated with the tip approaching the prism surface demonstrates the tip-apex region as the origin of the resonance peak.

the form of second harmonic generation (SHG) from the apex region of the tips.

SHG is forbidden in the dipole approximation for media with inversion symmetry [137]. In scattering geometry, for sagittal illumination and tip-parallel polarization, the SHG response from the tip is then dominated by the apex region, where the macroscopic translational invariance is broken in the axial direction. With the symmetry being radially conserved, little signal is expected from the conical near-apex shaft area [138]. For the experiments, linearly polarized incident light from a mode-locked Ti:sapphire oscillator (pulse duration < 15 fs, $\lambda = 805$ nm) is directed onto the sharp end of the free standing tip and the scattered SHG signal is spectrally selected and detected.

The contribution of the local field-enhancement of SHG from the metal tips is derived comparing the signal strength obtained with that of a planar surface of the same material. With the SH-enhancement expected to be dominated by the tip apex, a SH-enhancement of $\sim 5 \times 10^3 - 4 \times 10^4$ was observed for Au tips with $r \simeq 20$ nm. With the SH-power $\propto E^4$ [139] this corresponds to an amplification of 8 – 25 for the average electric field near the apex, in agreement with estimates based on other SHG experiments [140]. For W tips significantly lower values for the SH enhancement are found corresponding to local field factors between 3 and 6. These results are also in good agreement with theoretical models, despite microscopic variations in the details of the tip geometry, as discussed below.

The excitation of the localized surface plasmon polariton (SPP) in the axial direction is responsible for the field enhancement observed experimentally for Au tips. A systematic investigation of the influence of these geometric parameters in terms of cone angle and tip radius would be highly desirable; however, the limitations due to the electrochemical preparation procedure render this difficult.

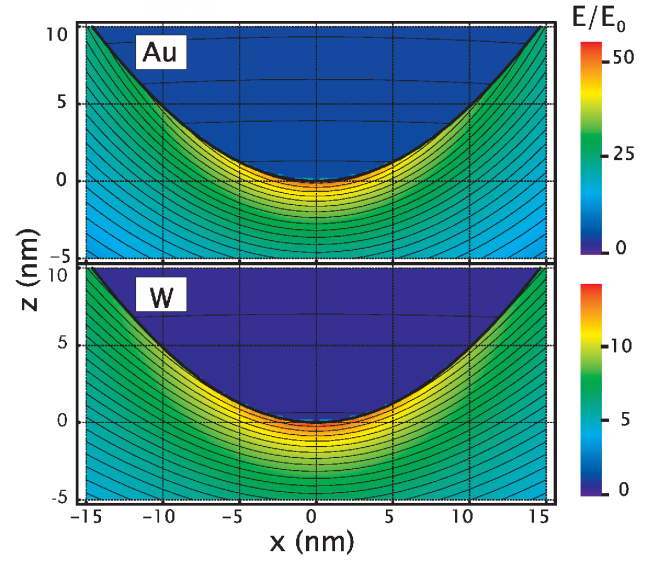


Figure 5: Dependence of field enhancement (E/E_0) on tip material for free standing tips with apex radius $r = 10$ nm, and wavelength of $\lambda = 630$ nm. The solid lines represent contours of constant potential [95].

5. Calculation of the near-field distribution at the tip-apex

The near-field distribution and enhancement has been derived for a variety of tip model geometries and tip and sample material combinations using different theoretical methods [81, 92, 95, 130, 132, 141, 142, 143, 144] (and references therein). The accurate theoretical treatment of the problem involves the solutions of Maxwells equations. This can be performed numerically for a chosen model tip-geometry [94, 131, 145, 146]. Although this may closely reproduce the experimental observations, the approach is computationally very demanding. It has remained difficult to extract the underlying relevant microscopic parameters responsible for the optical response observed, given that the effects of tip geometry, tip material, tip-sample distance, and optical field are coupled.

Taking advantage of the small dimensions of the tip apex compared to the optical wavelength ($kr \ll 1$, with k the wave vector and r the tip-apex radius), the problem can be treated in the quasistatic approximation which allows solving the Laplace equation analytically for certain geometries [95, 130, 132, 142, 143, 144] to derive the local field distribution [87, 147]. With the size of the apex region with $r \sim 10$ nm this implies that the electric field has the same amplitude and phase across the structure at any time and thus retardation effects can be neglected [133, 148]. Despite constraints in terms of tip geometries which can be treated in that approach, in contrast to purely numerical techniques this method provides direct insight into how the solutions scale with several experimentally relevant structural and material parameters.

Here, we represent the tip as a hyperboloid and the influence of different dielectric and structural parameters on the

near-field enhancement and distribution is systematically derived for both bare tips and tip-sample systems [95]. The optical wavelength dependance is explicitly taken into account considering the frequency dependence of the dielectric functions of tip and sample media [149].

Fig. 5 shows characteristic local field distributions and the corresponding enhancement near the apex region of free standing tips of gold (a) and tungsten (b). The equipotential surfaces are indicated by solid lines. In both cases the radius of the apex and the cone semiangle are fixed to $r = 10$ nm and to $\theta = 20^\circ$, respectively. Setting the incident light at a wavelength of $\lambda = 630$ nm and polarized along the tip axis, this closely resembles the conditions in the TERS experiments.

At optical frequencies, even for metals as tip material, the tip surface does not represent an equipotential surface, in contrast to the pure electrostatic case. The finite response time of the charge carriers with respect to the optical frequency results in the decay of the field inside the tip on the length scale given by the skin depth. For gold as a representative material with high conductivity this results in the strongest field enhancement of $E/E_0 \approx 50$ at the apex [150]. In contrast, tungsten as a common scanning probe tip material, is a poor conductor in the optical frequency range leading to a comparably moderate enhancement of ~ 12 . The degree of field enhancement E/E_0 at the tip apex depends sensitively on apex radius and cone semiangle, due to their influence on the plasmon resonance as discussed briefly below and in [95]. In general, values range between 10 and 100 for typical gold tips with 10 – 20 nm radius and realistic semiangles.

Despite the necessary approximations inherent to the quasistatic approach, the theoretical results presented here prove to be sufficiently accurate for most practical purposes. This is drawn from comparison with the experimental results shown above. From the tip-scattered SHG experiments the local field enhancement of 8 – 25 for Au and 3 – 6 for W was estimated for $r = 20$ nm apex radii. Considering that the experimental enhancement factors presented above are obtained as an spatial average over the apex region, these values fall well within the range of the theoretically predicted enhancements given in Fig. 5.

6. Tip-sample optical coupling

The local field enhancement as well as the lateral confinement can change significantly for the tip in close proximity to a surface plane. This behavior is of crucial importance for the optical contrast in scattering near-field microscopy. The optical tip-sample coupling is the result of the forcing of the boundary conditions at the surface plane on the field emerging from the apex. With the incident electric field inducing an optical dipole excitation in the tip, the presence of the sample can be accounted for by considering a virtual image dipole located inside the sample, with the resulting field distribution being a superposition of the fields of the two dipoles [151]. This gives rise to a mutual and constructive tip-sample optical polarization when the electric field is oriented parallel with respect to the tip axis (p -polarized). For an s -polarized incident field, the

tip - dipole is induced parallel to the sample surface, and the correspondent image - dipole aligned antiparallel. This leads to a partial cancellation and hence reduced field intensity and scattering [58].

Fig. 6 (top panel) displays the evolution of the field in the tip-sample gap calculated along the axial direction for different distances d for a Au tip approaching a flat Au sample. As can be seen, the tip-sample approach is accompanied by a significant increase in field enhancement in the tip-sample gap. The tip-sample interaction is correlated with apex radius and becomes significant at distances below about twice the tip radius (here, $d = 20$ nm) when the near-field interaction becomes effective, with a particularly fast rise of the field at the sample surface. It reaches values of up to several hundred for $d = 2$ nm showing an increase of more than one order of magnitude when compared with the free standing tip. In addition, the field enhancement with decreasing tip-sample distance is accompanied by a strong lateral confinement of the field underneath the apex [95]. The equipotential surface is forced to align close to parallel with the substrate plane which gives rise to an enhanced lateral concentration of the field.

The enhancement is strongly dependent on the sample material, being most pronounced for metallic substrates. Simultaneously, the lateral confinement also varies with the sample, *i.e.*, decreases with decreasing the material optical polarizability of the material. This is important as it leads to an increased spatial resolution in scanning probe near-field microscopy for small tip-sample distances, as discussed in [95].

One of the virtues of the quasistatic model is the direct access to the spectral variation of the field distribution for different tip-sample geometries. The spectral tip-scattered response can become a complex superposition of the tip and the sample optical properties, the understanding of which is important in nano-spectroscopy.

For a Au tip ($r = 10$ nm) approaching a Au surface Fig. 6 (bottom panel) shows the calculated spectral dependance of the field enhancement near the surface. As expected, a structural plasmon resonant behavior is observed. Associated with the increase in field enhancement for shorter distances a spectral shift in the plasmon response to longer wavelengths is observed. This red shift is especially pronounced for distances $d \leq r$, *i.e.*, correlated with the onset of the sharp rise in field enhancement as discussed above and a manifestation of the regime of strong coupling. Spectral peak widths of order 0.2 to 0.3 eV correspond to what is expected from the electronic dephasing times for SPP in Au of $\sim 10 - 20$ fs [152]. Using tungsten as tip material, no plasmon behavior is obtained, except for the case when it is combined with a sample that can sustain an SPP itself [95].

The determination of the field enhancement for a tip-sample coupled system has been experimentally achieved by TERS from surface monolayers of molecular adsorbates [73, 77, 81, 85, 94]. From tip-sample distance dependent Raman measurements in comparison with corresponding far-field experiments, using malachite green (MG) dye molecules or single-walled carbon nanotubes (SWCN) near-field enhance-

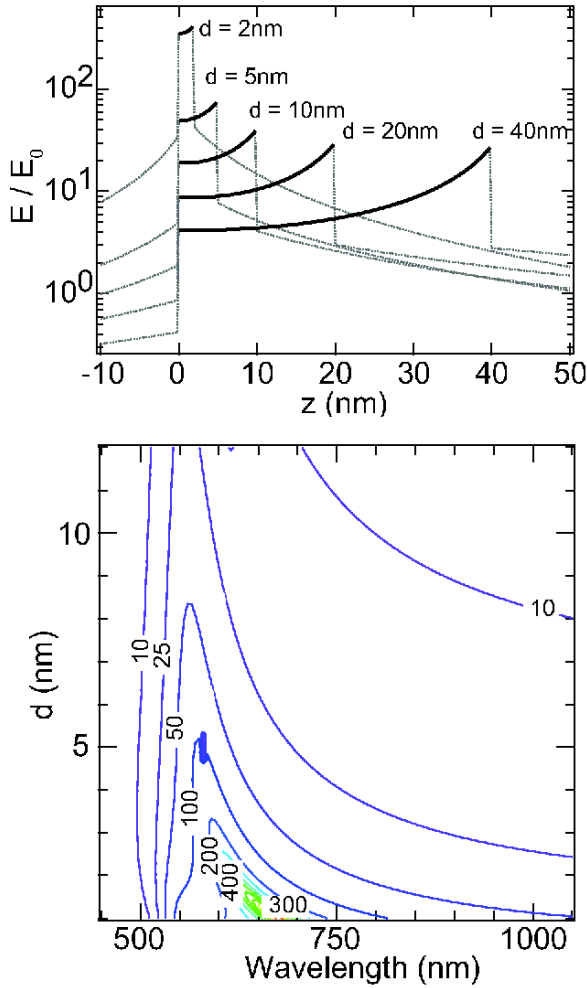


Figure 6: Top: Variation of field enhancement E/E_0 along the axial direction across the tip-sample gap region for different distances d for a Au tip ($r = 10$ nm) and Au sample at an excitation wavelength of $\lambda = 630$ nm. The tip is at variable $z = d$ positions and extends to the right. The sample surface is located at $z = 0$ nm and its bulk occupies the range of negative z -values. Bottom: Spectral dependance of field-enhancement with tip-sample distance d for a Au tip ($r = 10$ nm) approaching a Au surface. The pronounced red shift of the plasmon response is associated with the strong near-field tip-sample coupling for $d \leq r$. The lines represent contours of equal optical field enhancement [95].

ments of 60 - 150 at the sample surface were measured, as detailed below. These experimental values are in good agreement with the theoretical ones ranging from ~ 50 to ~ 300 as shown in Fig. 6 for small tip - sample distances.

The spectral characteristics of the plasmon response found in these calculations and shown in Fig. 6 display a red-shift for the case of a Au tip approaching a Au surface. It is the result of the superposition of the dielectric functions of the tip and the sample material mediated by the tip-sample optical coupling. This is a general phenomenon and it is found in calculations of spheres and other plasmonic nanostructures in

close proximity to a metal surfaces [132, 146, 153, 154], and has been observed experimentally in TERS and light emission in inelastic tunneling [155, 156, 157].

The field distributions and enhancement and their spectral dependence calculated within the quasistatic approximation for a hyperbolic tip are found to agree with other detailed theoretical observations. Using a fully 3D finite-difference time-domain (FDTD) method we have calculated the field distribution [94] with similar results obtained in [142, 146, 158]. The comparison with both the exact theoretical treatments and experimental results validates the approach of treating the probe tip in the quasistatic approach to a good approximation. Despite the simplicity of the model, the essential optical properties and the physical trends characteristic for the optical response of the the tip-sample system are accurately predicted.

7. Near-field character and far-field artifacts in TERS

TERS manifests itself in an enhancement of the Raman response, with the increase confined to the region underneath the tip-apex. However, with the illumination extended on a larger surface region determined by the far-field focus, the discrimination of the variation of far-field response due to the presence of the tip inside the focus is difficult in general [73].

Without any lateral scanning or systematic vertical tip-sample distance variations this in general does not allow for the unambiguous assignment of the observed optical effect to a near-field process. The apparent Raman signal rise may be due to far-field effects occurring when the tip is scanned inside the tight laser focus that can influence both signal generation and detection. With the tip penetrating into the focus region it would allow to scatter additional, otherwise forward-scattered (non-enhanced) far-field Raman light back into the detector. Furthermore, the interference of tip-scattered, surface reflected and incoming pump light results in locally enhanced pump intensities. With both processes affecting a surface region not confined by the apex area, they can dominate over the near-field effects.

In Fig. 7 tip-scattered Raman results are shown for single-wall carbon nanotubes (SWCN) and monolayers (ML) of malachite green (MG) molecules with the tip in force feedback at $d = 0$ nm [159], versus tip retracted by several 100 nm. When the tip is within several nanometers above the sample surface, a strong increase in Raman intensity is observed for both adsorbates (spectra denoted $SWNT^{tip}$ and MG^{tip}). Note that the difference in noise level from the SWNT to the MG spectra is due to different spectral resolution settings of the spectrometer. Despite being frequently applied to assign the observed signal to TERS [112] simply comparing surface vs. tip scattered Raman intensities near- and far-field processes are *a priori* indistinguishable. The inset of Fig. 7 shows the Raman peak intensity as a function of the tip-sample distance obtained in two similar experiments for monolayers of MG molecules adsorbed on flat Au surface. The overall increase in signal is comparable in both cases, and an estimate of the Raman enhancement factor gives $G > 10^6$

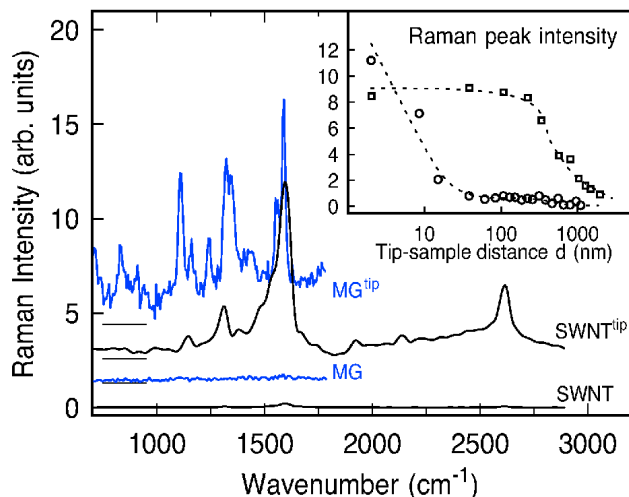


Figure 7: Near-field signature vs. far-field artifact: Raman spectra of single-walled carbon nanotubes and MG molecules with tip retracted (SWNT, MG) and tip engaged (SWNT^{tip}, MG^{tip}). Inset: tip-sample distance dependence of the Raman signal obtained under similar conditions but displaying very different behaviors: the ~ 20 nm length scale increase is characteristic for the near-field signal origin (circles); the few hundred nanometer decay length (squares) shows a far-field artifact - leading to similar signal increase as the near-field response. Dashed lines added as guide for the eye.

(*vide infra*). However, with the distance variation occurring on a length scale correlated with pump wavelength or focus dimensions, in one case the enhancement can solely be attributed to far-field effect (squares). A true near-field effect manifests itself in a correlation of the spatial signal variation with the tip radius (~ 20 nm). Here, with high quality tip (sharp apex, smooth tip shaft), the near-field contribution can dominate the overall signal (circles). Therefore for the tip-scattered Raman signal only the demonstration of a clear correlation of the lateral or vertical tip-molecule distance dependence with tip radius allows for an unambiguous near-field assignment of the optical response [73], as is true for all near-field microscopies including *s*-SNOM and the special case of TERS [16, 19, 59, 65].

Experimental quantification of the near-field Raman enhancement

In contrast to SERS where the quantification of the enhancement is a difficult task in general, for the tip-scattering experiment, the Raman enhancement factor can be derived from comparison of tip-enhanced versus far-field response of the same surface monolayer. Fig. 8 shows the spectrally resolved tip-scattered Raman signal during approach of ~ 1 ML of MG on gold (2 nm/step, 1 s/spectrum acquisition time). The pump light is polarized along the tip axis (p^m) and the Raman signal is detected unpolarized. Although a faint Raman signature of the molecules is observed with the tip at $d > 100$ nm, a clear molecular fingerprint is obtained only when the tip is within

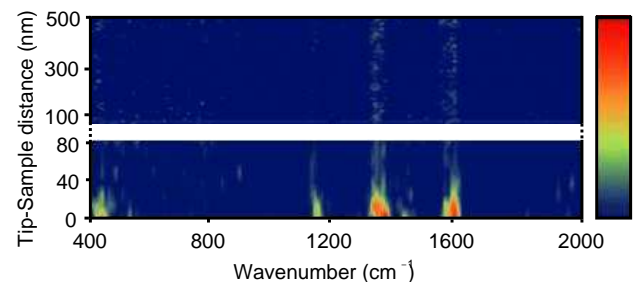


Figure 8: Tip-sample distance dependence of spectrally resolved Raman signal during approach of ~ 1 ML of MG on gold. Each spectrum is acquired for 1 s and the approach is realized with 2 nm increments. Near-field tip-enhanced signal is observed with the tip within ~ 20 nm above the sample, displaying typical Raman modes for MG molecules [81].

~ 20 nm from the sample. The prominent bands around 1615 cm^{-1} and 1365 cm^{-1} are assigned to combinations of the C=C stretching vibrations of the phenyl ring and the mode at 1170 cm^{-1} is due to a methyl group rocking mode or an in-plane C-H bending mode of the phenyl ring [160].

The enhancement is confined to a tip-sample spacing of just several nanometers and correlated with the apex radius of the tip, as expected for the near-field signature. The increase in Raman response is accompanied by a weak rise in a spectrally broad fluorescence background that has been subtracted. With the molecular fluorescence being quenched due to the electronic coupling to the metal substrate, this emission could largely be attributed to the enhancement of the intrinsic tip luminescence in conjunction with excitation of plasmonic modes in the tip-sample cavity [155, 161], *i.e.*, its origin is independent of the molecular adsorbates.

With the near-field character of the Raman response verified, the experimental field-enhancement factor can be derived from comparison of the tip-enhanced versus far-field response from the same surface monolayer. For the experiments presented here, the integrated Raman signal over the $1150 - 1650\text{ cm}^{-1}$ spectral region is used after background subtraction.

As shown in Section 5, the electromagnetic near-field enhancement originates from a sample surface area approximated by the area of the tip apex [73]. For the evaluation of the enhancement factor, the different areas probed in the near-field (TERS) and far-field (FF) cases are then taken into account. For the TERS setup, the illumination focus has a diameter $d \simeq (\lambda / \text{N.A.}) \times 1.5 = 1.7\text{ }\mu\text{m}$ (the 1.5 factor accounts for the deviation of the laser beam from a perfect gaussian profile). Considering the $\sim 70^\circ$ angle of incidence of the pump light with respect to the surface-normal in our setup, the actual surface region illuminated is elongated elliptically and larger, with a total area of $\sim 27\text{ }\mu\text{m}^2$. In the case of the confocal-Raman setup (FF) used to record the far-field spectrum of MG, the same laser illuminates an area of 870 nm^2 . Using the inter-atomic distances the molecule is estimated to occupy a surface area of $\sim 0.87\text{ nm}^2$ (actual 3D spatial filling: $1.18\text{ nm} \times 1.39\text{ nm} \times 0.98\text{ nm}$). 1 ML surface coverage then

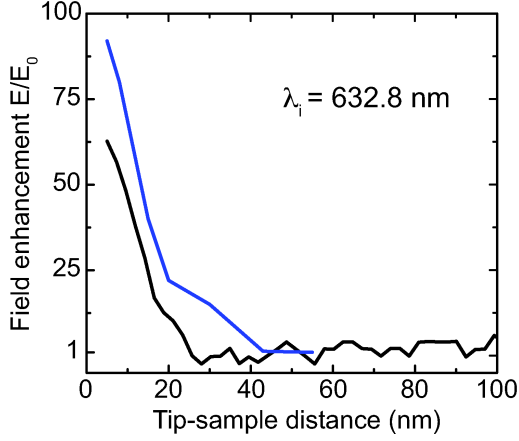


Figure 9: Field enhancement (E/E_0) for two different Au tips approaching ~ 1 ML of MG on gold. The Raman response is integrated over the $1150 - 1650 \text{ cm}^{-1}$ spectral region after background subtraction and the enhancement factors are calculated according to $I_{\text{TERS}} \propto E^4$.

corresponds to approximately 10^6 molecules are in the focus of the far-field setup and only < 200 are responsible for the tip-enhanced signal for a tip with 10 nm apex radius.

In addition to the areas, the detection efficiencies for the two different experimental arrangements are considered. The far-field response is emitted only in half space ($\Omega = 2\pi$) assuming an isotropic dipolar intensity pattern, and with N.A. = 0.9 a total of $\sim 27\%$ of the Raman signal is detected, in contrast to the TERS experiments with $\sim 2\%$ for N.A. = 0.35 and assuming the emission pattern following a $\cos^2(\theta + \frac{\pi}{2})$ dependence ($\theta \in [0, \pi]$).

Taking all these factors into consideration, the Raman enhancement factor can be estimated, and is found to range from 10^6 to 10^9 with variation mostly depending on the tip used. This enhancement is expected to be purely electromagnetic in origin. Here the molecule experiences the tip-enhanced local-field $E_{\text{loc}}(v_i) = L(v_i) E(v_i)$, with $L(v_i)$ the enhancement factor of the incident field $E(v_i)$. The concomitant enhancement of the polarization $P(v_s)$ at the Raman-shifted frequency v_s is $L'(v_s)$. Therefore, the total field enhancement is given by $L(v_i) \cdot L'(v_s)$ [93, 139]. With the Raman intensity $I \propto |L(v_i) \cdot L'(v_s) \cdot E(v_i)|^2$, the total Raman enhancement factor G is given by $G = |L(v_i) \cdot L'(v_s)|^2$ [162]. Although different in general, the field enhancement factors $L(v_i)$ and $L'(v_s)$ for pump and Raman polarizations, respectively, can be assumed to be similar in this case [163, 164]. This is motivated by both the spectrally broad plasmonic resonance of the tip and its red-shift upon approaching the sample surface [95, 132, 165].

Fig. 9 shows the effective field enhancement factors ($L(v_i) \cdot L'(v_s) = E/E_0$) for the integrated Raman signal from ~ 1 ML of MG on gold as a function of tip-sample distance for two different Au tips (both with $r < 15$ nm). Maximum enhancements of ≥ 90 and ≥ 60 (black and blue curves, respectively) are obtained considering variation of the tip-scattered

Raman response with the forth power of the electrical field, as indicated above. The molecules adsorbed on the planar Au surface already experience a field enhancement given by the Fresnel factor [166]. We will therefore also derive the total enhancement with respect to the free molecule response.

The study of the polarization dependence of the Raman response offers additional insight into the electromagnetic enhancement of TERS. Fig. 10 shows near-field Raman spectra from ~ 1 ML of MG on gold for the different polarization combinations of both pump and Raman light. Incident laser power and acquisition times are identical for all spectra. The polarization directions are defined as parallel (p) and perpendicular (s) with respect to the plane of incidence formed by the incoming wave vector $k(\omega_i)$ and the tip axis. No background has been subtracted and the data are normalized with respect to the intensity of the 1615 cm^{-1} mode measured in $p^{\text{in}}/p^{\text{out}}$ configuration (upper left panel).

With the incident field polarized perpendicular on the tip axis (s^{in}), almost no Raman signal is observed, irrespective of the polarization of the scattered light. In contrast, with the pump polarized along the tip axis (p^{in}), clear Raman fingerprints of MG molecules are observed with the Raman response being predominantly polarized parallel to the tip ($p^{\text{in}}/p^{\text{out}}$) as expected for near-field TERS from isotropically distributed molecules with diagonal Raman tensor components as the case of MG. For both $s^{\text{in}}/p^{\text{out}}$ $p^{\text{in}}/s^{\text{out}}$ configuration, weak overall signal is observed due to the absence of the tip-sample optical coupling. For $s^{\text{in}}/s^{\text{out}}$ a larger background is observed, albeit with no Raman enhancement, as expected.

The highly polarized TER response observed in our experiments indicates the absence of significant near-field depolarization, for the homogeneous and slender tip geometries used. This is required for symmetry selective probing in TERS and other nonlinear tip-enhanced processes [167, 168, 169, 170] that rely on polarization selective and conserving light scattering. In contrast, for a Ag particle-topped quartz AFM probe as used for probing the 520 cm^{-1} Raman band of Si [171] the observed Raman depolarization has been attributed to the wide cone angle of the tip [119].

8. TERS of molecular adsorbates

In Fig. 11 representative tip-enhanced Raman spectra are shown for MG on smooth Au surfaces. They are taken for the same surface coverage of ~ 1 ML, but using different tips exhibiting enhancements of 3×10^8 (a), 7×10^7 (b), 1×10^7 (c), and 1×10^6 (d), respectively. The experimental uncertainty is estimated at a factor of 3 – 5 for each value. The tip-enhanced Raman spectra are reproducible for a given tip. But, as seen from the data, the spectral details vary from tip to tip. With the lateral confinement of the tip-enhancement within a ~ 10 nm diameter surface region and a molecular density of $\sim 1/\text{nm}^2$ we estimate that the signal observed in Fig. 11 a) - d) originates from ~ 100 molecules.

In the lower panel of the figure the far-field Raman spectrum from the same sample is shown for comparison (black line). The far-field spectrum closely resembles that in aqueous

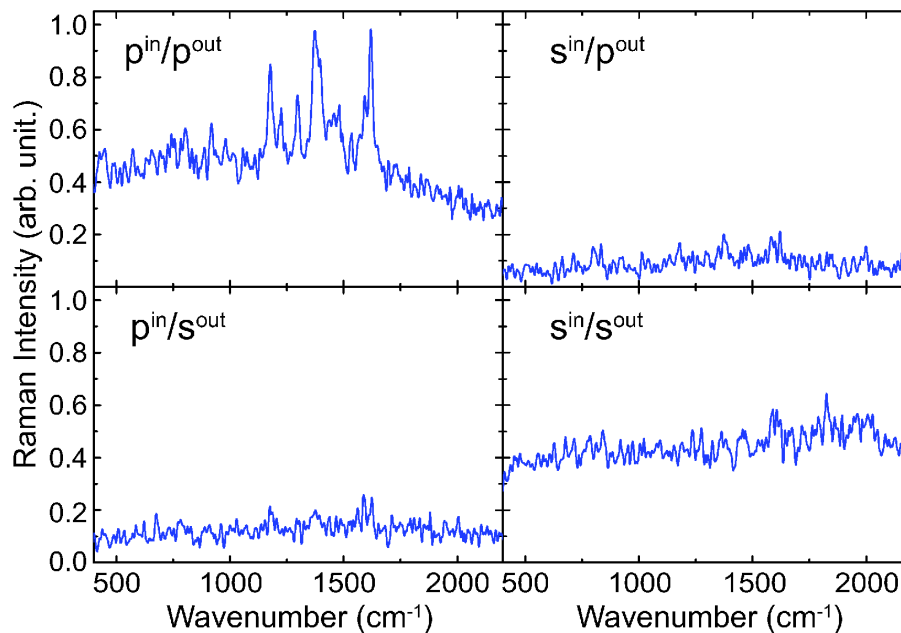


Figure 10: Polarization dependence of the near-field tip-enhanced Raman response originating from ~ 1 ML of MG on gold. All spectra are acquired for the same time and normalized to the maximum intensity value of the 1615 cm^{-1} mode in $p^{in} - (\text{unpol.})^{out}$ geometry. Very weak Raman response is observed with the pump polarized perpendicular on the tip axis (s^{in}), in contrast with the case of (p^{in}), where strong near-field coupling gives rise to Raman enhancement. The spectrally broad background is due to intrinsic luminescence from the Au tip itself.

solution [160] indicating that the molecules are physisorbed in isotropic orientation at the surface. The blue bars represent normal Raman modes of the MG anion calculated using density functional theory as implemented in Gaussian03 as discussed in [81]. The assignment and spectral position of the calculated modes agree well with literature values [160, 172].

For moderate near-field enhancements $\leq 10^7$, both spectral positions and relative intensities of the modes resemble the far-field signature, as seen in Fig. 11 c) and d) and in accordance with other TERS results for similar enhancement [79]. However, with increasing enhancement of 7×10^7 (b), and most pronounced for 3×10^8 (a), the vibrational modes start to look markedly different. While some of the modes are present in both, far-field and near-field spectra (e.g., 920 cm^{-1} , 1170 cm^{-1} , and 1305 cm^{-1}), some other are only present in the highly enhanced near-field results (e.g., 1365 cm^{-1} , 1544 cm^{-1}). The vertical dashed lines in Fig. 11 are added as a guide to the eye for easier comparison.

The DFT calculation allows for the identification of the spectral features in the far-field data of Fig. 11. The majority of the intense Raman modes can be attributed to modes either localized at the phenyl ring or delocalized over the two dimethylamino phenyl groups. In the spectral region of 910 cm^{-1} to 980 cm^{-1} several vibrational modes, typically characterized by in-plane skeletal bending and/or out-of-plane C—H motions, are found. The 1170 cm^{-1} mode may be assigned to a methyl group rocking mode or an in-plane C—H bending mode of the phenyl ring. Around 1300 cm^{-1} in-plane C—H deformation modes and C—C stretching modes of the methane group are located.

Furthermore, the calculations show that the new spectral features seen in the highly enhanced near-field spectra in Fig. 11 mostly correspond to vibrational normal modes of MG. Among the characteristic near-field enhanced modes, e.g., the peak at 1365 cm^{-1} , which is very strong in the far-field spectrum, but decreases with increasing enhancement, can be assigned to combination of the C=C stretching motions of the aromatic ring. In contrast, the prominent peak at 1544 cm^{-1} which dominates for the highest enhancement is very weak for small enhancements or in the far-field spectra. Here, the calculation shows a mode characterized by stretching motions combined with in-plane C—H bending motions of the conjugated di-methyl-amino-phenyl rings. The two modes at 1585 and 1615 cm^{-1} , which can be assigned to C=C stretching vibrations of the phenyl ring, decrease with enhancement.

This change in both intensity and spectral signature with increasing near-field enhancement together with the vibrational analysis shows that the peaks observed may well correspond to vibrational modes of MG, whereby different selection rules must apply for the Raman spectra obtained under condition of high enhancements [162].

In the following we discuss possible physical mechanisms leading to the experimental observations. Due to the high localization of the optical near-field, the molecules in the tip-sample gap experience a large field gradient and different Raman symmetry selection rules can come into play [173, 174, 175]. This Gradient Field Raman effect (GFR) [176] and the mechanism by which strong field gradients can influence the molecular Raman spectra by altering the selection rules require that the polarizability tensor (α_{ab}) and

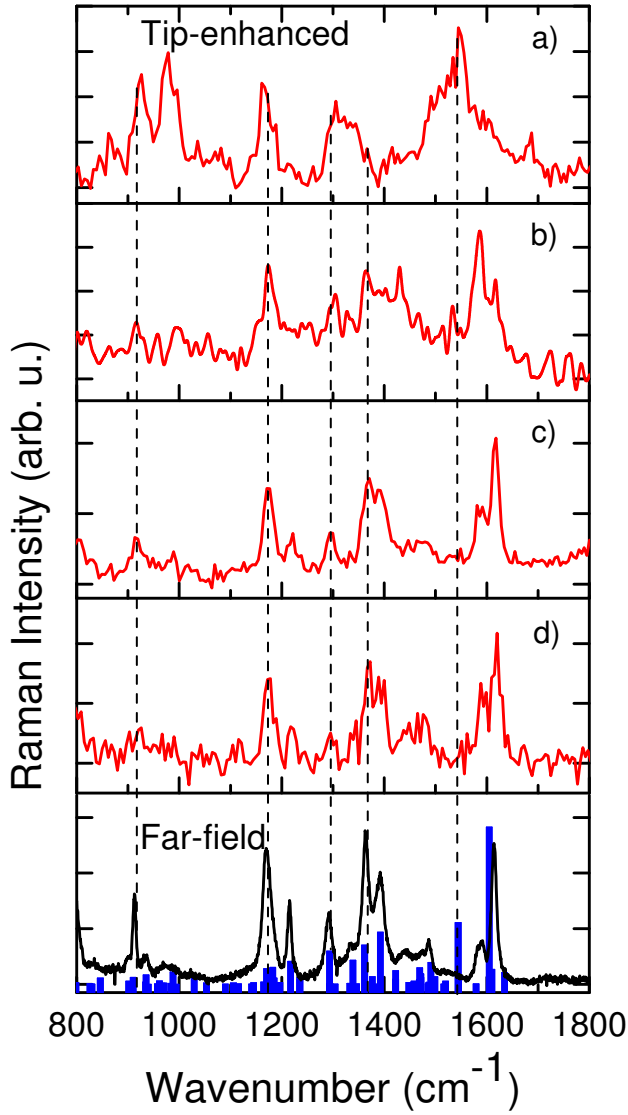


Figure 11: Tip-enhanced Raman spectra for ~ 1 ML of MG for different degrees of enhancement (a,b,c,d) in comparison with the corresponding far-field Raman spectrum (bottom graph) and DFT calculation for the mode assignment (blue bars). The Raman enhancement factors derived are 3×10^8 (a), 7×10^7 (b), 1×10^7 (c), and 1×10^6 (d), respectively. Data are acquired for 1 s (a), 100 s (b,c), and 30 s (d), respectively. Spectral resolution is 25 cm^{-1} for the near-field and 1 cm^{-1} for the far-field spectra [96].

$(dE_b/dQ)_{Q=0}$ must simultaneously be nonzero [176], where E is the electric field, Q the vibrational coordinate and $a, b \in \{x, y, z\}$. The resulting selection rules resemble the surface selection rules [177], and give rise to GFR spectral lines which complement the Raman spectra. The presence of the field gradient may also lead to IR modes becoming Raman active [176]. In the case of MG, it was verified that the few IR modes show no noticeable resemblance with the highly enhanced TER spectra (details in [81]). While it is difficult to quantify the contribution of GFR in general [176], strong circumstantial evidence from the occurrence of normally for-

bidden modes, akin the observation in the TERS results suggest that the process contributes in this case. Similar differences between far- and near-field Raman spectra were reported previously in fiber-based SNOM experiments on Rb-doped KTiOPO_4 [20, 21].

In addition, the optical field gradient can also couple to vibrations via the derivative of the quadrupole polarizability A_{ijk} of a mode ($\propto \partial A_{ijk} / \partial Q \nabla E$) [175]. With α_{ab} and A_{ijk} transforming differently in terms of symmetry and their ratio being highly mode dependent this could also account for the mode selectivity observed in tip-enhanced Raman scattering. However, the DFT calculations of A_{ijk} are still deemed challenging for large molecules yet they would be desirable and can contribute to a unified description of the underlying processes, given the well characterized structural environment in tip-enhanced Raman in contrast to most SERS experiments. It might also help to resolve the striking observation that the strength of the calculated four modes at 846, 988, 1029, and 1544 cm^{-1} are overestimated by DFT calculation as compared to the far-field spectra, but coincidentally represent modes that are relatively strongly enhanced in the TER spectra.

The pronounced spectral differences between the tip-enhanced and far-field Raman response resemble observations made in SERS, where vibrational modes which are normally not Raman allowed had been found [178, 179, 180]. Aside from orientational effects, these spectral variations are typically interpreted to arise from conformational changes and/or transient covalent binding of the molecule at "active sites" [177]. With that being unlikely in the tip-enhanced Raman geometry discussed here, this could indicate that purely electromagnetic mechanisms might already induce the kind of spectral selectivity observed in our TERS experiments.

9. Molecular bleaching

An important question regarding the appearance of different spectral features in the near-field tip-enhanced Raman spectra is the influence of the molecular bleaching or other decomposition products [181, 182]. With the molecules under investigation exposed to the strongly localized and enhanced near-field, this leads to a sometimes rapid photo-decomposition process, especially in a resonant Raman excitation.

To probe for the possible appearance of photoreaction products and their signature in the Raman spectra the evolution of the Raman emission is monitored in time-series experiments. Fig. 12 (left panel) shows consecutive near-field Raman spectra acquired for 1 s each for an enhancement of 1.3×10^7 with an incident laser fluence of $3 \times 10^4 \text{ W/cm}^2$. The molecules bleach on a time scale of ~ 100 s, depending on the enhancement level, and the decay and subsequent disappearance of the spectral response is uniform, *i.e.*, the relative peak amplitudes are maintained. During the bleaching no new spectral features appear from possible photoreaction products and the signal decays with the relative peak amplitudes remaining constant. After complete bleaching no discernible Raman response can be observed. The fluctuation observed in the time series is expected given the small number of ~ 100 molecules probed in

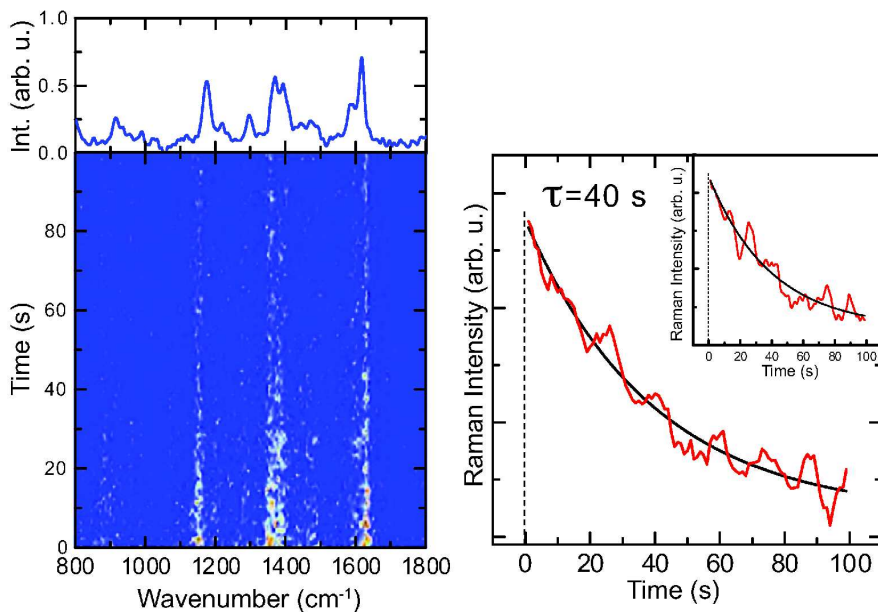


Figure 12: Left: Time series of 100 consecutive near-field Raman spectra (acquired for 1 s each) for ~ 1 ML MG on Au (Raman enhancement 1.3×10^7). The signal decays to zero due to bleaching and no new spectral features appear from the photoreaction products. The sum Raman spectrum (top panel) clearly resembles the far-field spectrum. Right: Bleaching kinetics derived for the spectrally integrated Raman time series and the region from 1550 to 1650 cm^{-1} (inset) [96].

the near-field enhanced region under the tip apex. The sum over all spectra (top graph) or the sum of any large enough subset even at later times, *i.e.*, after substantial bleaching has already occurred, closely resembles the far-field response of MG and thus allows to attribute the Raman response to MG molecules.

The same behavior of a gradual and homogeneous disappearance of the Raman response without a relative change in peak intensity is also observed for larger enhancements, *i.e.*, the case where a different mode structure is observed. However, the larger local field experienced by the molecules leads in general to decreasing decay time constants.

Fig. 12 (right panel) shows the decay kinetics of the spectrally integrated Raman intensity for the time series data shown on the left. This is shown in comparison to the integral intensity of the region from 1550 to 1650 cm^{-1} encompassing only the two prominent modes (inset). Assuming an exponential decay behavior of $I/I_0 = \exp(-t/\tau)$ for the Raman intensity a decay time $\tau = 40 \pm 5$ s is derived from the fit in both cases (solid lines). From the applied laser fluence of 3×10^4 W/cm^2 and the enhancement of the pump intensity of $\sim \sqrt{1.3 \times 10^7}$ the bleaching would be induced by a local pump fluence of 4.7×10^7 W/cm^2 .

An extreme case of molecular bleaching is shown in Fig. 13. A time series of 100 consecutive Raman spectra from a sample with submonolayer molecular coverage, with each spectrum acquired for 1 s is recorded. The estimated Raman enhancement factor is 9×10^7 and the spectral features deviate from the far-field Raman spectrum presented in

Fig. 11 b, akin to the ones shown in the same figure panels a) and b) for high enhancement level (*e.g.*, the mode at 1544 cm^{-1}). After an illumination time of about 50 s, the overall Raman intensity drops suddenly over the whole spectral region, and most visible for the peak at 1306 cm^{-1} . With this being a strong indication that the probed molecules undergo a bleaching process, it is interesting to note that no new spectral features emerge. Thus even for extreme cases as the one presented here, the molecular decomposition products do not contribute to the observed Raman signal. It was suggested that the molecular bleaching rate could be used for the derivation of the enhancement factor [112]. It should be noted that the bleaching rate is not a characteristic physical quantity universal for a given molecule. For example, malachite green isothiocyanate - a sister dye of MG - was found to bleach with a rate constant more than two orders of magnitude higher than the MG studied here [112], if renormalized to the same experimental conditions. Bleaching mechanisms can be quite diverse [183]. They may include irreversible photoinduced or even multi-photon induced reactions such as rearrangements, dissociation and fragmentation, elimination or hydrogen abstraction or perhaps photooxidation with ambient oxygen via triplet states. It can depend on, *e.g.*, humidity or cleanliness of tip and sample, and is hence not a useful measure to compare experiments performed under different conditions in different laboratories.

With the experiments carried out under ambient conditions, special care must be taken to use clean samples and tips. It is well known [184] that contaminating carboniferous species

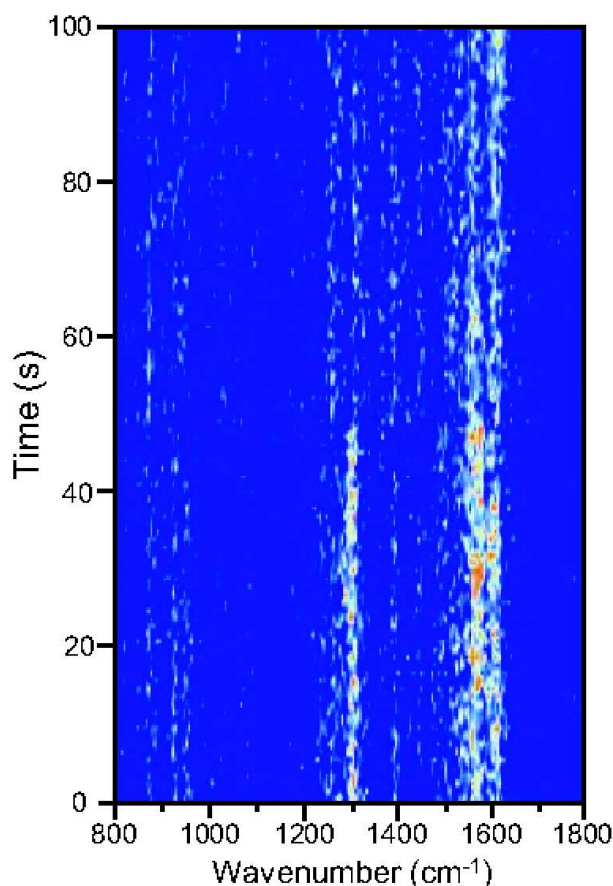


Figure 13: Time series of 100 NF Raman spectra acquired for 1 s each. After ~ 50 s the Raman intensity reduces due to bleaching, but no signature of secondary products is visible.

and/or carbon clusters can adhere to either tip or sample and reveal their Raman signature in the tip-enhanced spectra, *e.g.*, Raman bands of appreciable intensity at frequencies above 1750 cm^{-1} [185].

A carboniferous Raman response (see Fig. 6 in [96]) manifests itself in characteristic spectral features from carbon clusters much different from the spectral response discussed above for monolayer or submonolayer MG. In accordance with previous observations [184, 185, 186], the carbon Raman response is comparatively large and fluctuates rapidly in an uncorrelated way. In contrast to the data on MG, a distinct spectral feature emerges around 2000 cm^{-1} which has been assigned to, *e.g.*, modes within the segments of carbon chains [185], and which is absent in the TER spectra of MG. This absence of the carbon Raman response can be understood since the bleaching of monolayer and submonolayer MG coverage leads to smaller molecular fragments and subsequently to a dilute surface carbon distribution and hence does not lead to extended carbon chains and aggregates which can readily form by multilayer MG decomposition at ambient temperatures.

Besides the degradation of the analyte, another potential source of carbon contamination is the near-field probe itself.

At room temperature and in a non-controlled atmosphere, contamination molecules from the environment could stick to the tip surface and reveal highly enhanced Raman signals. TERS control experiments with the bare tip and clean Au samples prior to MG deposition were carried out to confirm the absence of vibrational Raman signature. Only intrinsic tip luminescence could be observed in that case [81].

10. TERS with single molecule sensitivity

With the measured tip-enhanced Raman spectra presenting a signal-to-noise ratio of more than 40:1 when probing ~ 100 molecules for 1 s accumulation time, this demonstrates the potential for even single molecule sensitivity. For the subsequent experiment we resort to a sample prepared with submonolayer surface coverage, adjusted to expect on average < 1 molecule under the tip-confined area of $\sim 100\text{ nm}^2$.

Corresponding near-field tip-enhanced Raman spectra measured in a time series with 1 s acquisition time for each spectrum are shown in Fig. 14 (left panel). Here the tip has been held at a constant distance $d = 0\text{ nm}$ above the sample and the total Raman enhancement is estimated at 5×10^9 [159]. The observed Raman signal exhibits temporal variations of relative peak amplitudes and fluctuations in spectral position. These are characteristic signatures of probing a single emitter in terms of an individual molecule. Similar observations have been made before in SERS [37, 38, 39, 41] with the fluctuations in the spectroscopic signature of a single emitter typically attributed to changes in its local environment, its structure, molecular diffusion [36, 187], and changes in molecular orientation [182]. With MG only physisorbed, it has to be considered in particular that the molecules can diffuse in and out of the apex-confined probe region while experiencing different degrees of enhancement. The diffusion dynamics can be facilitated by the thin water layer present on the sample surface under ambient conditions.

In the time series in Fig. 14 the apparent bleaching rate seems reduced compared to what is expected from the analysis of the ensemble bleaching discussed above. This is a result of the low surface coverage where new molecules directly neighboring the tip-sample gap can diffuse into the near-field enhanced region. However, the signal vanishes rapidly after 100 s due to the eventual depletion after the molecules surrounding the near-apex area have bleached.

A different mode structure of MG is observed compared to the far-field response - highly visible for the $1500 - 1600\text{ cm}^{-1}$ spectral region, akin to the results for strong enhancements shown above. Fig. 14 (middle panel) displays the sum spectrum (olive) for the single molecule response time series (left) in comparison with ensemble spectra of ~ 100 molecules probed for one second (red) showing different degrees of enhancement: 3×10^8 in a) and 7×10^7 in b). Panel c) presents the sum spectrum (blue) of the data shown in Fig. 12 a) which, as for a moderate enhancement, closely resembles the far-field spectrum. The resemblance of the Raman spectrum of a molecular ensemble with the sum spectrum over the whole time series offers strong evidence of probing sin-

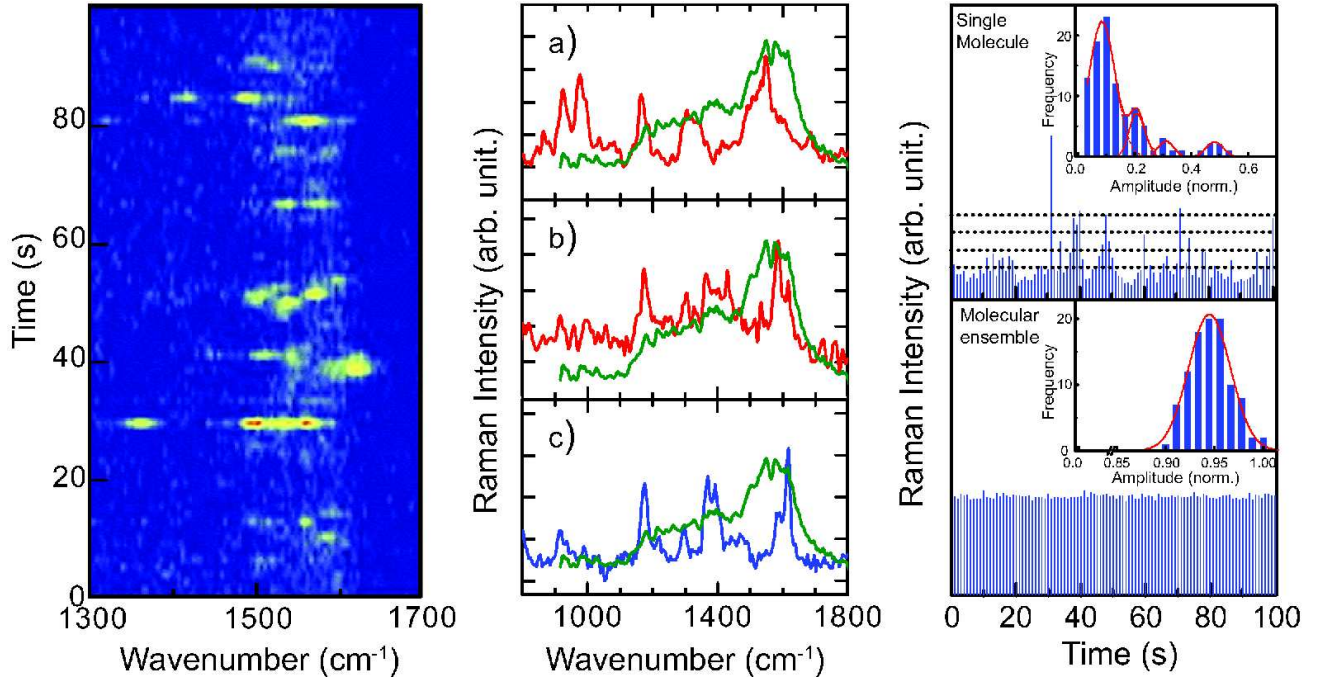


Figure 14: Left: Time series of tip-scattered Raman spectra for a sub-monolayer MG surface coverage with Raman enhancement of 5×10^9 . The spectral diffusion observed is characteristic for observing single MG molecules. Middle: Comparison between sum spectrum of data shown in left panel (olive) and tip-enhanced Raman spectra for different degrees of enhancement (red, a) and b)) and sum spectrum of data shown in Fig. 12 (blue). Right: Temporal variation of the Raman intensity of the integrated 1480 - 1630 cm^{-1} of time series shown in left panel (top). From the corresponding histogram (inset) a discretization of Raman intensities can be seen with 170-230 $\text{counts} \cdot \text{molecule}^{-1} \cdot \text{s}^{-1}$ (dashed line increment). For comparison, temporal variation of the Raman intensity of the integrated 1480 - 1630 cm^{-1} of big molecular ensemble (far-field) is shown (bottom) together with corresponding histogram (inset) [81, 96].

gle intact MG molecules [40]. Note that the sum over the times series shall therefore resemble an ensemble spectrum for large enhancement, rather than the far-field Raman spectrum. In assessing the resemblance of the spectral characteristics it has to be considered that at low coverage the molecules have more degrees of freedom to dynamically change orientation and they can diffuse. Given the rather weak response, the signal detected can only be expected to emerge from the region of largest enhancement, and with the diffusing molecules probing the spatial variation of the enhancement under the tip this corresponds to an extreme case of inhomogeneous broadening. Therefore, while individual spectral features at positions in accordance with the strongly tip-enhanced near-field response are observed in the time series, the sum spectrum no longer exhibits clearly resolved lines. This interpretation is further sustained considering, *e.g.*, the improved resemblance of the peak in the 1550 - 1600 cm^{-1} region of the single molecule sum spectrum with the sum of the two near-field spectra (in a and b) of different enhancement.

Further insight is obtained by studying the statistical behavior of the single molecule Raman response [36]. Fig. 14 (right panel top graph) displays the integrated 1430 cm^{-1} to 1650 cm^{-1} spectral intensity for the data in the left panel. The signal intensities cluster with intervals of 170-230 $\text{counts} \cdot \text{s}^{-1}$, as already evident from visually inspecting the time-series of

integrated intensities (dashed lines), and this manifests itself in the corresponding histogram in an asymmetric distribution with discrete peaks (inset). This behavior is qualitatively reproducible for experiments with the same surface coverage and it can be interpreted as the Raman emission from $n = 0$ (noise peak), 1, 2, and 3 molecules being probed under the tip, as suggested for similar findings in SERS [34, 36]. This assignment is corroborated from experiments with different surface coverages: for lower coverages only the $n = 0$ and 1 peaks remain and with increasing coverage the distribution converges to a narrow random Gaussian distribution which is observed from a large molecular ensemble, as seen in the lower panel, where 100 consecutive far-field spectra were acquired for 100 s each and the signal is integrated over the same spectral range as in the case of the single molecule experiment. The details of the histogram, however, depend on the binning procedure especially for a small data set as has been shown to be insufficient as the sole argument for single molecule observation [188].

The optical trapping and alignment of MG under the tip must also be considered as a possible source of the observed surface diffusion and intensity fluctuations [189]. However, for MG together with our particular experimental conditions, this can not explain the discretization of Raman peak intensities in the single molecule response, as detailed elsewhere

[81].

Our single molecule TER results are similar to other recent experimental findings [85] where brilliant cresyl blue molecules adsorbed on planar Au were probed. For enhancements of $\sim 10^7$ similar to our intermediate values, temporal fluctuations in both intensity and mode frequency were observed, albeit with no significant spectral differences between the far-field and near-field response as seen here for high enhancements.

11. Raman imaging of nanocrystals: Near-Field Crystallographic Symmetry

TERS can provide symmetry selective information. This potential, however, has yet been largely unexplored. Here we show that the characteristic symmetry properties of the tip scattering Raman response in terms of independent control of polarization and k vector for both incident and Raman scattered light provides the necessary degree of freedom to determine the crystallographic orientation and -domains in nanostructures. This is due to the fundamental interaction with lattice phonons of the Raman process, together with the symmetry properties and selection rules of the tip-enhanced scattering that allows for identifying crystallographic axes without requiring atomic resolution. With Raman scattering being less invasive than electron or x-ray techniques and applicable *in situ*, this approach will fill a much needed gap in the characterization of nanostructured materials with increasing complexity [190, 191].

Transmission Electron Microscopy, capable of providing atomic resolution [192], requires samples thin enough to be transparent for electrons, extensive sample preparation, and due to vacuum conditions, makes *in situ* experiments difficult [193]. Likewise, X-ray microscopy is capable of characterizing nanostructures with atomic resolution [194], but requires a monochromatic brilliant synchrotron radiation source and radiation beam damage remains a concern [195]. Here, the comparable simplicity of TERS from an instrumentation perspective makes it highly attractive providing complementary information and even avoiding some of the disadvantages of the existing techniques.

In Raman spectroscopy, the specific phonon modes probed depend on the chosen experimental geometry, in terms of the incident and detected polarization as well as the propagation direction of light [5, 196]. These phonon modes allow determination of the crystallographic orientation of a sample. This has been shown in far-field Raman in, *e.g.* the study of 90° domain switching in bulk BaTiO_3 [197] or the observation of ferroelastic domains in LaNiO_4 [198]. However, in Raman microscopy, in the commonly used confocal epi-illumination and detection geometry, this reduces the available degrees of freedom, and thus losing the general capability of probing the symmetry specific Raman tensor elements. In extending the use of the Raman selection rules to a side-illuminated TERS geometry, these degrees of freedom can be regained and even further refined by taking into account the tip geometry as discussed in the following.

The intensity of the Raman scattered light from a medium is given by: $I_s \propto |\vec{e}_s \cdot \vec{R} \cdot \vec{e}_i|^2$ where \vec{e}_i and \vec{e}_s are the polarization of the incident and scattered light, respectively and the Raman tensor \vec{R} is the derivative of the susceptibility tensor [199]. As an example, for a Raman-active phonon mode of tetragonal BaTiO_3 , \vec{R} is given by:

$$\mathbf{A}_1(\vec{\xi}) = \begin{pmatrix} a & 0 & 0 \\ 0 & a & 0 \\ 0 & 0 & b \end{pmatrix}$$

where $\vec{\xi}$ denotes the polarization direction of the mode (for polar modes). The symmetry of a given mode, in this case A_1 , is determined from group theory and may contain multiple component phonon modes of different frequency [200]. Thus, when the polarization conditions, determined from the susceptibility derivative, are satisfied for a given symmetry mode, the Raman shift due to the phonons belonging to that mode can be observed.

In addition, one can selectively isolate specific phonon modes within a symmetry mode. For polar modes, the phonons will separate into Transverse Optical (TO) and Longitudinal Optical (LO) components [201], which, being distinct in frequency, can be spectrally resolved. This is not accounted for by the Raman tensor methods described above, requiring further refinement of the selection rules.

For a given geometry, the wavevector \vec{q} of the propagating phonon can be determined by conservation of momentum from the wavevectors of the incident and scattered light. Based on the relative orientation between \vec{q} and $\vec{\xi}$, one can selectively excite the LO mode for $\vec{q} \parallel \vec{\xi}$, or the TO mode for $\vec{q} \perp \vec{\xi}$. Thus, the observation of either a TO or an LO mode provides the additional information about the orientation of the crystallographic axes.

Furthermore, drawing on the nanoscopic apex of a plasmonic tip for preferential enhancement of incident light polarized along the tip axis allows us to exploit the unique symmetry selection rules associated with the tip [92]. This will enhance modes whose polarizations coincide with this axis. Therefore we expect maximum enhancement of modes for which both allowed incident and scattered polarization directions are oriented parallel with the tip axis. Modes for which either the incident or scattered polarization coincide with the enhancement axis may also be observed, albeit with a lower intensity.

The potential for applying the symmetry properties of the Raman selection rules in a tip-enhanced geometry has been emphasized previously [119, 202, 203, 204]. However, no general treatment has yet been discussed. Here we will briefly summarize the essential elements for tip-enhanced Raman spectroscopy of nanocrystals, with further details to be published elsewhere [205].

In order to demonstrate the conceptual capability of TERS on nanocrystals, we studied individual single crystal BaTiO_3 nanorods in the tetragonal phase [206]. Perovskite BaTiO_3 , a displacive ferroelectric at room temperature, has long been

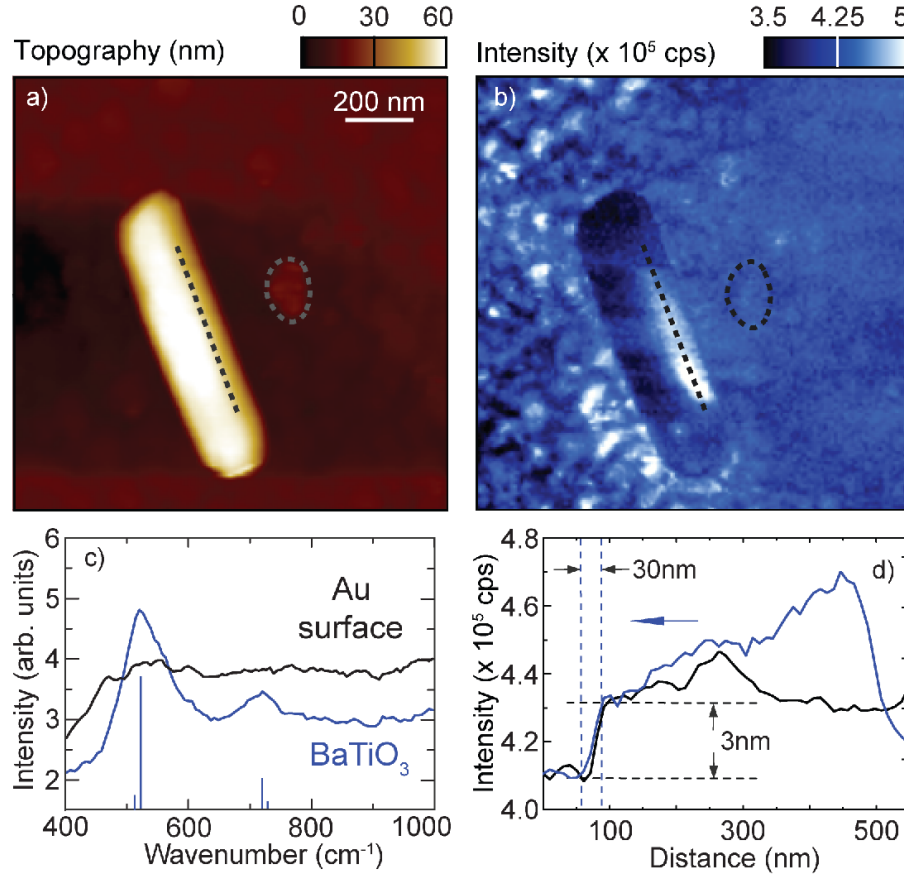


Figure 15: a) Shear-force topography of a crystalline BaTiO₃ nanorod on a Au substrate ($1.28 \times 1.28 \mu\text{m}^2$). b) Spectrally integrated TERS signal from the same surface region, showing strong optical contrast on top of the nanorod, as well as above highly localized substrate regions. The enclosed region (dashed line) shows low signal enhancement due to dielectric contrast from sample contamination. c) Raman spectra acquired on a BaTiO₃ rod (blue) and on Au substrate (black). The peaks are identified (blue vertical lines) as E₁ TO mode at 510 cm^{-1} , a second order peak at 520 cm^{-1} and a combination of the A₁ LO and E₁ LO modes at 727 cm^{-1} and 715 cm^{-1} , respectively. A cross section of the region of high enhancement (blue) and corresponding topography (blue) on the rod is shown in panel d), taken as an average over 3 adjacent pixels along the straight dashed line in panels a) and b). The strong rise in optical signal (left) is correlated with a $\sim 3 \text{ nm}$ height variation, unlike the sharp decrease in optical response (right) which has no topographic correspondent; this seems to indicate the presence of a crystal defect.

the focus of intense study due to interest in these properties [207]. Although ferroelectric domain formation and crystallographic orientation on the macroscale are well understood, complementary studies on the nanoscale are desired.

TERS acquired from a BaTiO₃ rod is shown in Fig. 15. The BaTiO₃ nanorods were placed on a Au-coated quartz substrate. Panel a) shows the shear-force topography of a rod, with the corresponding spectrally integrated TERS signal acquired simultaneously in panel b). The incident polarization is parallel to the tip axis and the detected signal is unpolarized with an acquisition time of 10 ms for each pixel.

On the Au substrate itself, topographically localized regions (down to 30 nm) can be identified, of intense luminescence enhancement due to the plasmonic tip-sample coupling [155]. These regions are correlated with small nanometer-scale Au surface features. In contrast, the enclosed area in the figure shows a clear topography but a comparatively weak enhancement of the optical signal. This suggests a surface

contamination resulting in dielectric contrast but little or no plasmonic coupling.

Panel a) shows TERS spectra acquired on top of a nanorod (blue) and on the Au substrate (black). The peaks at 520 cm^{-1} and 720 cm^{-1} identify the material as BaTiO₃ and can be assigned to a higher order peak and a combination of the A₁ LO and E₁ LO modes, respectively [196]. The spectral positions and estimated relative intensities of the peaks are shown by the vertical lines underneath the curve. The spectrally broad luminescence background observed originates from the Au tip itself.

Panel d) shows cross section profiles taken from panels a) and b) (black and blue, respectively). Spatial resolution of 30 nm can be estimated and is correlated with tip apex. The cross section is taken from the region of strong Raman enhancement on the rod, as indicated by the straight dashed lines in a) and b). The signal shown is the average over 3 consecutive pixels disposed orthogonal to the cross-sectional direction. A

clear correlation between a 3 nm rise in the topography with a strong increase in the optical signal can be seen. This indicates a distinct region of the rod responsible for the increased signal. Due to distinct topographic features of BaTiO₃ previously observed at grain boundaries [208], we attribute the signal observed in this region to different crystallographic subdomains in the rod [209].

Although the study of nanocrystalline samples opens up a wide range of potential applications for TERS, some fundamental aspects are not yet fully understood. Recent far-field studies of wurtzite CdS nanorods indicate a possible depolarization effect in dielectric nanostructures, leading to a breaking of the Raman tensor selection rules [210]. Furthermore, it has been shown that the presence of a sharp edge within the near-field of a photoemitter can affect the polarization of the emitted light [211], although the resulting effect on Raman scattering is yet unclear. In addition, the large field gradient near the tip can fundamentally alter the selection rules, making previously silent modes visible [176]. Although this may render IR and other modes Raman-active [212], making mode assignment more difficult, this would shed further insight into the fundamental material properties.

12. Outlook

Reproducibility can be enhanced performing TERS under controlled experimental environmental conditions. Performing experiments under *e.g.*, Ultra High Vacuum (UHV) conditions offers variable sample temperature and combination with other UHV techniques for surface analysis [82, 156]. Tip enhanced Raman spectroscopy may emerge as an important analytical tool for chemical and structural identification on the nanoscale. It offers chemical specificity, nanometer spatial resolution, single molecule sensitivity and symmetry selectivity. However, with both sensitivity and spatial resolution critically dependent on the well defined geometry and related optical properties of the tip, reproducibility has remained an issue in TERS. Furthermore, for direct far-field illumination conditions, it is difficult to *a priori* distinguish the near-field response from the unspecific far-field imaging artifacts (*vide supra*).

Future developments in tip design and fabrication may prove critical. We have recently demonstrated a novel way to generate a nanoconfined light emitter on a nanoscopic probe tip obtained by grating-coupling of surface plasmon polaritons on the tip-shaft [213]. The adiabatic field concentration of the propagating SPP, determined by the boundary conditions imposed by the tapered shape of the tip, offers an intrinsic nanofocusing effect and thus gives rise to confined light emission only from the apex region, as theoretically predicted [214].

In this experiment linear gratings are written onto the shaft of Au tips by focused ion beam milling, $\sim 10\ \mu\text{m}$ away from the apex, as schematically shown in Fig. 16 a). Upon grating illumination with a broadband light source (150 nm spectral bandwidth of Ti:sapphire oscillator), SPP are excited and launched towards the apex [152, 215], where they are re-radiated, as shown in Fig. 16 b) (details discussed in [213]).

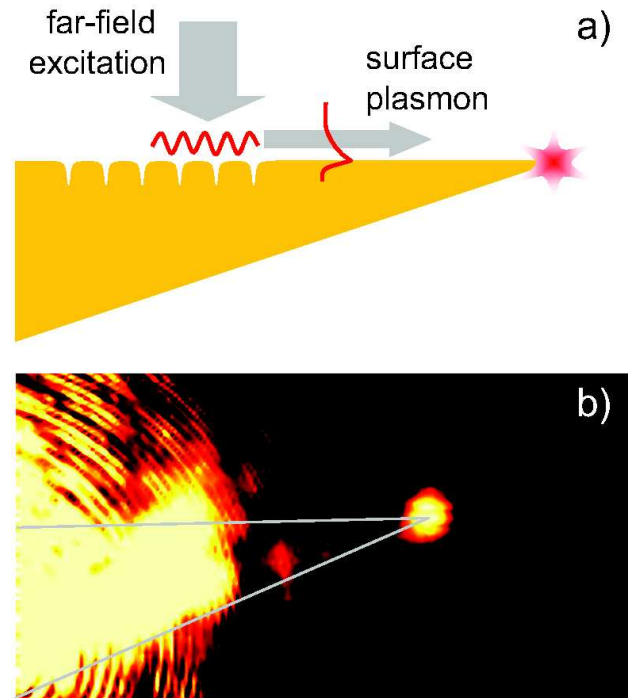


Figure 16: a) Principle of the nonlocal excitation of the tip apex. Far-field radiation excites SPP on the grating, which propagate along the shaft towards the tip apex, where they are reradiated into the far-field. b) Microscope image recorded for illumination of the tip-grid demonstrating the efficient nonlocal excitation of the tip apex via illumination of the grating [213].

Spatially separating the excitation from the apex itself, this approach is particularly promising as it avoids the otherwise omnipresent far-field background present for direct apex illumination. In addition, it would provide the spatial resolution needed for near-field optical techniques including *s*-SNOM and TERS.

13. Summary

A systematic understanding both experimentally and theoretically of the fundamental processes responsible for field enhancement, spectral tip plasmonic response and tip-sample coupling has allowed for reaching Raman enhancement factors as high as 10^9 leading to the ultimate sensitivity limit in analytical spectroscopy – the single molecule. With lateral resolution solely determined by the tip apex radius, nanometer spatial resolution can be obtained. Criteria have been discussed for experimental TERS implementation and distinction of near-field signature from far-field imaging artifacts. The combination of the inherent sensitivity and spatial resolution of TERS with the Raman selection rules and the unique symmetry of the scanning tip makes possible the spatially resolved vibrational mapping on the nanoscale. Its implementation for determining the orientation and domains in crystallographic nanostructures has been proposed. Future developments in tip design and more efficient illumination and detection geometries and scanning probe

implementation will allow for TERS to become a powerful nano-spectroscopic analysis tool.

Acknowledgment. The authors would like to thank Nicolas Behr, Jens Dreyer, Thomas Elsaesser, Christoph Lienau and Claus Ropers for valuable discussions and support, and Stanislaus Wong for providing the BaTiO₃ sample. Funding by the Deutsche Forschungsgemeinschaft through SFB 658 ("Elementary Processes in Molecular Switches at Surface"), the National Science Foundation (NSF CAREER grant CHE 0748226) is greatly acknowledged. S. B. thanks the National Science Foundation for the IGERT Fellowship.

-
- [1] Chalmers J, Griffiths P (Eds): *Handbook of Vibrational Spectroscopy*. John Wiley and sons, Chichester 2002.
 - [2] Kuzmany H: *Solid-State Spectroscopy*. Springer 1998.
 - [3] Wilson EB, Decius JC, Cross PC: *Molecular Vibrations: The Theory of Infrared and Raman Vibrational Spectra*. Dover 1980.
 - [4] Hendra PJ, Stratton PM: **Laser-Raman spectroscopy**. *Chem. Rev.* 1968, **69**:325.
 - [5] Hendra PJ, Vear CJ: **Laser Raman spectroscopy: A review**. *The Analyst* 1970, **95**:321.
 - [6] Yu PP, Cardona M: *Fundamentals of Semiconductors*. Springer, 3rd edition 2005.
 - [7] Aroca R: *Surface-Enhanced Vibrational Spectroscopy*. John Wiley & sons, Ltd 2006.
 - [8] Demtröder W: *Laser Spectroscopy: Basic Concepts and Instrumentation*. Springer, 2nd edition 1996.
 - [9] Tabaksblat R, Meier RJ, Kip BJ: **Confocal Raman microspectroscopy: Theory and application to thin polymer samples**. *Appl. Spectr.* 1992, **46**:60.
 - [10] Abbe E: **Beitrage zur Theorie des Mikroskops und der mikroskopischen Wahrnehmung**. *Archiv f. Mikroskop. Anat.* 1873, **9**:413.
 - [11] Strutt (Lord Rayleigh) J: **On the theory of optical images, with special reference to the microscope**. *Phil. Mag.* 1896, **42**:167.
 - [12] Lewis A, Isaacson M, Muray A, Harootunian A: **Scanning optical spectral microscopy with 500Å resolution**. *Biophys.J.* 1983, **41**:405a.
 - [13] Pohl DW, Denk W, Lanz M: **Optical stethoscopy: Image recording with resolution $\lambda/20$** . *Appl. Phys. Lett.* 1984, **44**:651.
 - [14] Lewis A, Isaacson M, Harootunian A, Muray A: **Development of a 500 spatial resolution light microscope. light is efficiently transmitted through $\lambda/16$ diameter apertures**. *Ultramicroscopy* 1984, **13**:227.
 - [15] Fillard J: *Near Field Optics and Nanoscopy*. World Scientific, Singapore 1997.
 - [16] Courjon D: *Near-Field Microscopy and Near-Field Optics*. Imperial Coll. Press, London 2003.
 - [17] Kawata S, Ohtsu M, Irie M: *Nanooptics*. Springer Verlag, New York 2002.
 - [18] Novotny L, Stranick SJ: **Near-field optical microscopy and spectroscopy with pointed probes**. *Annu. Rev. Phys. Chem.* 2006, **57**:303.
 - [19] Novotny L, Hecht B: *Principles of Nano-Optics*. Cambridge University Press 2006.
 - [20] Jahncke CL, Paesler MA, Hallen HD: **Raman imaging with near-field scanning optical microscopy**. *Appl. Phys. Lett.* 1995, **67**:2483.
 - [21] Jahncke CL, Hallen HD, Paesler MA: **Nano-Raman spectroscopy and imaging with a near-field scanning optical microscopes**. *J. Raman Spectrosc.* 1996, **27**:579.
 - [22] Webster S, Batchelder DN, Smith DA: **Submicron resolution measurement of stress in silicon by near-field Raman spectroscopy**. *Appl. Phys. Lett.* 1998, **72**:1478.
 - [23] Serio MD, Mohapatra H, Zenobi R, Deckert V: **Investigation of the liquid-liquid interface with high spatial resolution using near-field Raman spectroscopy**. *Chem. Phys. Lett.* 2006, **417**:425.
 - [24] Fleischmann M, Hendra P, McQuillan A: **Raman-spectra of pyridine adsorbed at a silver interface**. *Chem. Phys. Lett.* 1974, **26**:163.
 - [25] Jeanmaire D, Van Duyne R: **Surface Raman spectroelectrochemistry. Part I. Heterocyclic, aromatic, and aliphatic amines adsorbed on the anodized silver electrode**. *J. Electroanal. Chem.* 1977, **84**:1.
 - [26] Albrecht M, Creighton J: **Anomalously intense Raman spectra of pyridine at a silver electrode**. *J. Am. Chem. Soc.* 1977, **99**:5215.
 - [27] Moskovits M: **Surface roughness and the enhanced intensity of Raman scattering by molecules adsorbed on metals**. *J. Chem. Phys.* 1978, **69**:4159.
 - [28] Gersten JI, Nitzan A: **Electromagnetic theory of enhanced Raman scattering by molecules adsorbed on rough surfaces**. *J. Chem. Phys.* 1980, **73**:3023.
 - [29] Gersten JI: **The effect of surface roughness on surface enhanced Raman scattering**. *J. Chem. Phys.* 1980, **72**:5779.
 - [30] Gersten JI: **Rayleigh, Mie, and Raman scattering by molecules adsorbed on rough surfaces**. *J. Chem. Phys.* 1980, **72**:5780.
 - [31] McCall SL, Platzman PM, Wolff PA: **Surface enhanced Raman scattering**. *Phys. Lett. A* 1980, **77**:381.
 - [32] Kerker M, Wang DS, Chew H: **Surface enhanced Raman scattering (SERS) by molecules adsorbed at spherical particles: errata**. *Appl. Opt.* 1980, **19**:4159.
 - [33] Gersten JI, Nitzan A: **Spectroscopic properties of molecules interacting with small dielectric particles**. *J. Chem. Phys.* 1980, **75**:1139.
 - [34] Willets KA, Van Duyne RP: **Localized surface plasmon resonance spectroscopy and sensing**. *Annu. Rev. Phys. Chem.* 2007, **58**:267.
 - [35] Otto A, Mrozek I, Grabhorn H, Akemann W: **Surface-enhanced Raman scattering**. *J. Phys: Condens. Matter* 1992, **4**:1143.
 - [36] Kneipp K, Wang Y, Kneipp H, Perelman LT, Itzkan I, Dasari RR, Feld MS: **Single molecule detection using surface-enhanced Raman scattering (SERS)**. *Phys. Rev. Lett.* 1997, **78**:1667.
 - [37] Nie S, Emory SR: **Probing single molecules and single nanoparticles by surface-enhanced Raman scattering**. *Science* 1997, **275**:1102.
 - [38] Xu H, Bjerneld EJ, Käll M, Börjesson L: **Spectroscopy of Single Hemoglobin Molecules by Surface Enhanced Raman Scattering**. *Phys. Rev. Lett.* 1999, **83**:4357.
 - [39] Bjerneld EJ, Johansson P, Käll M: **Single molecule vibrational fine-structure of tyrosine adsorbed on Ag nanocrystals**. *Single. Mol.* 2000, **1**:239.
 - [40] Weiss A, Haran G: **Time-dependent single-molecule Raman scattering as a probe of surface dynamics**. *J. Phys. Chem.* 2001, **105**:12348.

- [41] Dieringer J, Lettan R, Scheidt K, Van Duyne R: **A frequency domain existence proof of single-molecule surface-enhanced Raman Spectroscopy.** *J. Am. Chem. Soc.* 2007, **129**:16249.
- [42] Michaels AM, Jiang J, Brus L: **Ag Nanocrystal Junctions as the Site for Surface-Enhanced Raman Scattering of Single Rhodamine 6G Molecules.** *J. Phys. Chem. B* 2000, **104**:11965.
- [43] Xu H, Aizpurua J, Käll M, Apell P: **Electromagnetic contributions to single-molecule sensitivity in surface-enhanced Raman scattering.** *Phys. Rev. E* 2000, **62**:4318.
- [44] Kneipp K, Kneipp H, Itzkan I, Dasari RR, Feld MS: **Ultra-sensitive chemical analysis by Raman spectroscopy.** *Chem. Rev.* 1999, **99**:2957.
- [45] Haynes C, Yonzon C, Zhang X, Van Duyne R: **Surface-enhanced Raman sensors: early history and the development of sensors for quantitative biowarfare agent and glucose detection.** *J. Raman Spectrosc.* 2005, **36**:471.
- [46] Aravind PK, Rendel RW, Metiu H: **A new geometry for field enhancement in surface-enhanced spectroscopy.** *Chem. Phys. Lett.* 1982, **85**:396.
- [47] Zenhausern F, O'Boyle MP, Wickramasinghe HK: **Apertureless near-field optical microscope.** *Appl. Phys. Lett.* 1994, **65**:1623.
- [48] Inouye Y, Kawata S: **Near-field scanning optical microscope with a metallic probe tip.** *Opt. Lett.* 1994, **19**:159.
- [49] Wessel J: **Surface-enhanced optical microscopy.** *J. Opt. Soc. Am. B* 1985, **2**:1538.
- [50] Fischer UC, Pohl DW: **Observation of single-particle plasmons by near-field optical spectroscopy.** *Phys. Rev. Lett.* 1989, **62**:458.
- [51] Specht M, Pedarnig JD, Heckl WM, Hänsch TW: **Scanning plasmon near-field microscopy.** *Phys. Rev. Lett.* 1992, **68**:477.
- [52] Bachelot R, Gleyzes P, Boccara AC: **Near-field optical microscope based on local perturbation of a diffraction spot.** *Opt. Lett.* 1995, **20**:1924.
- [53] Koglin J, Fischer UC, Fuchs H: **Material contrast in scanning near-field optical microscopy at 1-10 nm resolution.** *Phys. Rev. B* 1997, **55**:7977.
- [54] Sánchez EJ, Novotny L, Xie XS: **Near-field fluorescence microscopy on two-photon excitation with metal tips.** *Phys. Rev. Lett.* 1999, **82**:4014.
- [55] Keilmann F, van der Weide DW, Eickelkamp T, Merz R, Stöckle D: **Extreme sub-wavelength resolution with a scanning radio-frequency transmission microscope.** *Opt. Commun.* 1996, **129**:15.
- [56] Knoll B, Keilmann F: **Near-field probing of vibrational absorption for chemical microscopy.** *Nature* 1999, **399**:134.
- [57] Knoll B, Keilmann F: **Enhanced dielectric contrast in scattering-type scanning near-field optical microscopy.** *Opt. Commun.* 2000, **182**:321.
- [58] Raschke MB, Molina L, Elsaesser T, Kim DH, Knoll W, Hinrichs K: **Apertureless near-field vibrational imaging of block-copolymer nanostructures with ultrahigh spatial resolution.** *ChemPhysChem* 2005, **6**:2197.
- [59] **Tip enhancement.** In *Advances in nano-optics and nanophotonics*. Edited by ad V Shalaev SK, Elsevier 2007.
- [60] Kneipp K, Moskovits M, Kneipp H (Eds): *Surface-Enhanced Raman Scattering : Physics and Applications*. Topics in Applied Physics, Springer Berlin / Heidelberg 2006.
- [61] Rasmussen A, Deckert V: **New dimension in nano-imaging: breaking through the diffraction limit with scanning near-field optical microscopy.** *Anal. Bioanal. Chem.* 2005, **381**:165.
- [62] Novotny L: **The history of near-field optics.** *Progr. Opt.* 2007, **50**:137.
- [63] Krug II JT, Sánchez EJ, Xie XS: **Design of near-field optical probes with optimal field enhancement by finite difference time domain electromagnetic simulation.** *J. Chem. Phys.* 2002, **116**:10895.
- [64] Richards D, Milner RG, Huang F, Festy F: **Tip-enhanced Raman microscopy: practicalities and limitations.** *J. Raman Spectrosc.* 2003, **34**:663.
- [65] Kawata S: *Near-Field Optics and Surface Plasmon Polaritons*. Springer, Berlin 2001.
- [66] Stöckle RM, Suh YD, Deckert V, Zenobi R: **Nanoscale chemical analysis by tip-enhanced Raman spectroscopy.** *Chem. Phys. Lett.* 2000, **318**:131.
- [67] Anderson MS: **Locally enhanced Raman spectroscopy with an atomic force microscope.** *Appl. Phys. Lett.* 2000, **76**:3130.
- [68] Hayazawa N, Inouye Y, Sekkat Z, Kawata S: **Metallized tip amplification of near-field Raman scattering.** *Opt. Commun.* 2000, **183**:333.
- [69] Hayazawa N, Inouye Y, Sekkata Z, Kawata S: **Near-field Raman scattering enhanced by a metallized tip.** *Chem. Phys. Lett.* 2001, **335**:369.
- [70] Hayazawa N, Inouye Y, Sekkat Z, Kawata S: **Near-field Raman imaging of organic molecules by an apertureless metallic probe scanning optical microscope.** *J. Chem. Phys.* 2002, **117**:1296.
- [71] Anderson MS, Pike WT: **A Raman-atomic force microscope for apertureless-near-field spectroscopy and optical trapping.** *Rev. Sci. Instrum.* 2002, **73**:1198.
- [72] Hartschuh A, Anderson N, Novotny L: **Near-field Raman spectroscopy using a sharp metal tip.** *J. Microscop.* 2002, **210**:234.
- [73] Hartschuh A, Sánchez EJ, Xie XS, Novotny L: **High-resolution near-field Raman microscopy of single-walled carbon nanotubes.** *Phys. Rev. Lett.* 2003, **90**:095503.
- [74] Watanabe H, Ishida Y, Hayazawa N, Inouye Y, Kawata S: **Tip-enhanced near-field Raman analysis of tip-pressurized adenine molecule.** *Phys. Rev. B* 2004, **69**:155418.
- [75] Ichimura T, Hayazawa N, Hashimoto M, Inouye Y, Kawata S: **Tip-enhanced coherent anti-Stokes Raman scattering for vibrational nanoimaging.** *Phys. Rev. Lett.* 2004, **92**:220801.
- [76] Hayazawa N, Ichimura T, Hashimoto M, Inouye Y, Kawata S: **Amplification of coherent anti-Stokes Raman scattering by a metallic nanostructure for a high resolution vibration microscopy.** *J. Appl. Phys.* 2004, **95**:2676.
- [77] Pettinger B, Ren B, Picardi G, Schuster R, Ertl G: **Tip-enhanced Raman spectroscopy (TERS) of malachite green isothiocyanate at Au(111): bleaching behavior under the influence of high electromagnetic fields.** *J. Raman Spectrosc.* 2005, **36**:541.
- [78] Anderson N, Hartschuh A, Cronin S, Novotny L: **Nanoscale vibrational analysis of single-walled carbon nanotubes.** *J. Am. Chem. Soc.* 2005, **127**:2533.
- [79] Domke K, Zhang D, Pettinger B: **Toward Raman fingerprints of single dye molecules at atomically smooth Au(111).** *J. Am. Chem. Soc.* 2006, **128**:14721.
- [80] Verma P, Yamada K, Watanabe H, Inouye Y, Kawata S: **Near-field Raman scattering investigation of tip effects on C60 molecules.** *Phys. Rev. B* 2006, **73**:145416.
- [81] Neacsu CC, Dreyer J, Behr N, Raschke MB: **Scanning-probe Raman spectroscopy with single-molecule sensitivity.** *Phys. Rev. B* 2006, **73**:193406.
- [82] Steidtner J, Pettinger B: **High-resolution microscope for tip-**

- enhanced optical processes in ultrahigh vacuum. *Rev. Sci. Instr.* 2007, **78**:103104.
- [83] Hayazawa N, Watanabe H, Saito Y, Kawata S: **Towards atomic site-selective sensitivity in tip-enhanced Raman spectroscopy.** *J. Chem. Phys.* 2006, **125**:244706.
- [84] Neugebauer U, Roesch P, Schmitt M, Popp J, Julien C, Rasmussen A, Budich C, Deckert V: **On the way to nanometer-sized information of the bacterial surface by tip-enhanced Raman spectroscopy.** *ChemPhysChem* 2006, **7**:1428.
- [85] Zhang W, Yeo BS, Schmid T, Zenobi R: **Single molecule tip-enhanced Raman spectroscopy with silver tips.** *J. Phys. Chem. C* 2007, **111**:1733.
- [86] Jersch J, Demming F, Hildenhagen L, Dickmann K: **Field enhancement of optical radiation in the nearfield of scanning probe microscope tips.** *Appl. Phys. A* 1998, **66**:29.
- [87] Demming F, Jersch J, Dickmann K, Geshev PI: **Calculation of the field enhancement on laser-illuminated scanning probe tips by the boundary element method.** *Appl. Phys. B* 1998, **66**:593.
- [88] Klein S, Witting T, Dickmann K, Geshev P, Hietschold M: **On the field enhancement at laser-illuminated scanning probe tips.** *Single Mol.* 2002, **3**:281.
- [89] Mills DL: **Theory of STM-induced enhancement of dynamic dipole moments on crystal surfaces.** *Phys. Rev. B* 2002, **65**:125419.
- [90] Wu S, Mills DL: **STM-induced enhancement of dynamic dipole moments on crystal surfaces: Theory of the lateral resolution.** *Phys. Rev. B* 2002, **65**:205420.
- [91] Micic M, Klymyshyn N, Suh YD, Lu HP: **Finite element method simulation of the field distribution for AFM tip-enhanced surface-enhanced Raman scanning microscopy.** *J. Phys. Chem.* 2003, **107**:1574.
- [92] Neacsu CC, Reider GA, Raschke MB: **Second-harmonic generation from nanoscopic metal tips: Symmetry selection rules for single asymmetric nanostructures.** *Phys. Rev. B* 2005, **71**(20):201402.
- [93] Neacsu CC, Steudle GA, Raschke MB: **Plasmonic light scattering from nanoscopic metal tips.** *Appl. Phys. B* 2005, **80**(3):295.
- [94] Roth RM, Panoiu NC, Adams MM, Osgood RM, Neacsu CC, Raschke MB: **Resonant-plasmon field enhancement from asymmetrically illuminated conical metallic-probe tips.** *Opt. Expr.* 2006, **14**:2921.
- [95] Behr N, Raschke M: **Optical antenna properties of scanning probe tips: plasmonic light scattering, tip-sample coupling, and near-field enhancement.** *J. Phys. Chem. C* 2008, **112**:3766.
- [96] Neacsu CC, Dreyer J, Behr N, Raschke MB: **Reply to "Comment on 'Scanning-probe Raman spectroscopy with single-molecule sensitivity'".** *Phys. Rev. B* 2007, **75**:236402.
- [97] Anderson N, Anger P, Hartschuh A, Novotny L: **Subsurface raman imaging with nanoscale resolution.** *Nano Lett.* 2006, **6**(4):744–749.
- [98] Debus C, Lieb A, Drechsler A, Meixner AJ: **Probing highly confined optical field in the focal region of a high NA parabolic mirror with subwavelength spatial resolution.** *J. Microsc.* 2002, **210**:203.
- [99] Anger P, Feltz A, Berghaus T, Meixner AJ: **Near-field and confocal surface-enhanced resonance Raman spectroscopy at cryogenic temperatures.** *J. Microsc.* 2003, **209**:162.
- [100] Novotny L, Sánchez EJ, Xie XS: **Near-field optical imaging using metal tips illuminated by higher-order Hermite-Gaussian beams.** *Ultramicroscopy* 1998, **71**:21.
- [101] Novotny L, Beversluis MR, Youngworth KS, Brown TG: **Longitudinal field modes probed by single molecules.** *Phys. Rev. Lett.* 2001, **86**(23):5251–5254.
- [102] Karrai K, Tiemann I: **Interfacial shear force microscopy.** *Phys. Rev. B* 2000, **62**:13174.
- [103] Stipe BC, Mamin HJ, Stowe TD, Kenny TW, Rugar D: **Noncontact friction and force fluctuations between closely spaced bodies.** *Phys. Rev. Lett.* 2001, **87**:096801.
- [104] Gregor MJ, Blome PG, Schfer J, Ulbrich RG: **Probe-surface interaction in near-field optical microscopy: The nonlinear bending force mechanism.** *Appl. Phys. Lett* 1996, **68**:307.
- [105] Williamson RL, Brereton LJ, Antognozzi M, Miles MJ: **Are artefacts in scanning near-field optical microscopy related to the misuse of shear force?** *Ultramicroscopy* 1998, **71**:165.
- [106] Hoppe S, Ctistis G, Paggel JJ, Fumagalli P: **Spectroscopy of the shear force interaction in scanning near-field optical microscopy.** *Ultramicroscopy* 2005, **102**:221.
- [107] Karrai K, Grober RD: **Piezoelectric tip sample distance control for near field optical microscopes.** *Applied Physics Letters* 1995, **66**:1842.
- [108] Davy S, Spajer M, Courjon D: **Influence of the water layer on the shear force damping in near-field microscopy.** *Appl. Phys. Lett.* 1998, **73**:2594.
- [109] Okajima T, Hirotsu S: **Study of probe-surface interaction in shear-force microscopy: Effects of humidity and lateral spring constant.** *Opt. Rev.* 1998, **5**:303.
- [110] Durkan C, Shvets IV: **Investigation of the physical mechanisms of shear-force imaging.** *J. Appl. Phys.* 1996, **80**:5659.
- [111] Bernstein HJ, Buckingham AD: **Resonance Raman Spectra [and Discussion].** *Phil. Trans. R. Soc. London A, Math. Phys. Sci.* 1979, **293**:287.
- [112] Pettinger B, Ren B, Picardi G, Schuster R, Ertl G: **Nanoscale probing of adsorbed species by tip-enhanced Raman spectroscopy.** *Phys. Rev. Lett.* 2004, **92**:096101.
- [113] Guckenberger R, Hartmann T, Wiegraabe W, Bauneister W: *Scanning Tunneling Microscopy II.* Springer 1995.
- [114] Ibe J, Bey JP, Brandow S, Brizzolara R, Burnham N, Dilella D, Lee K, Marrian C, Colton R: **On the electrochemical etching of tips for scanning tunneling microscopy.** *J. Vac. Sci. Technol. A* 1990, **8**:3570.
- [115] Vasile MJ, Grigg DA, Griffith JE, Fitzgerald EA, Russell PE: **Scanning probe tips formed by focused ion beams.** *Rev. Sci. Instr.* 1991, **62**:2167.
- [116] Nam AJ, Teren A, Lusby TA, Melmed AJ: **Benign making of sharp tips for STM and FIM: Pt, Ir, Au, Pd, and Rh.** *J. Vac. Sci. Technol. B* 1995, **13**:1556.
- [117] Iwami M, Uehara Y, Ushioda S: **Preparation of silver tips for scanning tunneling microscopy imaging.** *Rev. Sci. Instr.* 1998, **69**:4010.
- [118] Ichimura T, Watanabe H, Morita Y, Verma P, Kawata S, Inouye Y: **Temporal fluctuation of tip-enhanced Raman spectra of adenine Molecules.** *J. Phys. Chem. C* 2007, **111**(26):9460–9464.
- [119] Ossikovski R, Nguyen Q, Picardi G: **Simple model for the polarization effects in tip-enhanced Raman spectroscopy.** *Phys. Rev. B* 2007, **75**:045412.
- [120] Kuhn S, Hkanson U, Rogobete L, Sandoghdar V: **Enhancement of single-molecule fluorescence using a gold nanoparticle as an optical nanoantenna.** *Phys. Rev. Lett.* 2006, **97**:017402.
- [121] Ren B, Picardi G, Pettinger B: **Preparation of gold tips suitable for tip-enhanced Raman spectroscopy and light emission by electrochemical etching.** *Rev. Sci. Instr.* 2004, **75**:837.
- [122] Picardi G, Nguyen Q, Schreiber J, Ossikovski R: **Compar-**

- ative study of atomic force mode and tunneling mode tip-enhanced Raman spectroscopy. *Eur. Phys. J. App. Phys.* 2007, **40**:197.
- [123] Klein M, Schwitzgebel G: **An improved lamellae drop-off technique for sharp tip preparation in scanning tunneling microscopy.** *Rev. Sci. Instr.* 1997, **68**:3099.
- [124] Wang X, Liu Z, Zhuang MD, Zhang HM, Wang X, Xie ZX, Wu DY, Ren B, Tian ZQ: **Tip-enhanced Raman spectroscopy for investigating adsorbed species on a single-crystal surface using electrochemically prepared Au tips.** *App. Phys. Lett.* 2007, **91**:101105.
- [125] Melmed A: **The art and science and other aspects of amking sharp tips.** *J. Vac. Sci. Technol. B* 1990, **9**:601.
- [126] Frankenthal RP, Thompson DE: **The anodic behavior of Gold in sulfuric acid solutions.** *J. Electrochem. Soc.* 1976, **123**:799.
- [127] Mao BW, Ren B, Cai XW, Xiong LH: **Electrochemical oscillatory behavior under a scanning electrochemical microscopic configuration.** *J. Electroanal. Chem* 1995, **394**:155.
- [128] Hillier J: **On the investigation of specimen contamination in the electron microscope.** *J. App. Phys* 1947, **19**:226.
- [129] Guise O, Ahner J, Yates J, Levy J: **Formation and thermal stability of sub-10-nm carbon templates on Si(100).** *App. Phys. Lett.* 2004, **85**:2352.
- [130] Denk W, Pohl DW: **Near-field optics: Microscopy with nanometer-size fields.** *J. Vac. Sci. Technol. B* 1991, **9**:510.
- [131] Novotny L, Bian RX, Xie XS: **Theory of nanometric optical tweezers.** *Phys. Rev. Lett* 1997, **79**:645.
- [132] Porto JA, Johansson P, Apell SP, Lpez-Ros T: **Resonance shift effects in apertureless scanning near-field optical microscopy.** *Phys. Rev. B* 2003, **67**:085409.
- [133] Bohren C, Huffman D: *Absorption and Scattering of Light by Small Particles.* Wiley, New York 1998.
- [134] Kretschmann E: **Untersuchungen zur Anregung und Streuung von Oberflaechenplasmaschwingungen an Silberschichten.** *PhD thesis*, University Hamburg 1972.
- [135] Leurgans P, Turner AF: **Frustrated totalinternal reflection interference filters.** *J. Opt. Soc. Am.* 1947, **37**:983.
- [136] de Fornel F (Ed): *Evanescent Waves.* Springer, Berlin 2001.
- [137] Heinz TF, Loy MMT, Thompson WA: **Study of Si(111) surfaces by optical second-harmonic generation: reconstruction and surface phase transformation.** *Phys. Rev. Lett.* 1985, **54**:63.
- [138] [In addition to the unique symmetry properties, the local surface and nonlocal longitudinal bulk polarizations contributions to the nonlinear polarization and their directional and polarization selection rules are directly distinguishable here due to the geometry of the tip as a partial asymmetric (∞mm) nanostructure with the mirror symmetry broken along the axis.].
- [139] Boyd RW: *Nonlinear Optics.* Academic Press, second edition 2003.
- [140] Ropers C, Neacsu CC, Raschke MB, Albrecht M, Lienau C, Elsaesser T: **Light confinement at ultrasharp metallic tips.** [Jap. J. App. Phys., in press].
- [141] Bouhelier A, Renger J, Beversluis MR, Novotny L: **Plasmon-coupled tip-enhanced near-field optical microscopy.** *J. Microsc.* 2003, **210**:220.
- [142] Festy F, Demming A, Richards D: **Resonant excitation of tip plasmons for tip-enhanced Raman SNOM.** *Ultramicroscopy* 2004, **100**:437.
- [143] Schneider SC, Grafstroem S, Eng LM: **Scattering near-field optical microscopy of optically anisotropic systems.** *Phys. Rev. B* 2005, **71**:115418.
- [144] Goncharenko AV, Dvoynenko MM, Chang HC, Wang JK: **Electric field enhancement by a nanometer-scaled conical metal tip in the context of scattering-type near-field optical microscopy.** *Appl. Phys. Lett.* 2006, **88**:104101.
- [145] Martin YC, Hamann HF, Wickramasinghe HK: **Strength of the electric field in apertureless near-field optical microscopy.** *J. Appl. Phys.* 2001, **89**:5774.
- [146] Downes A, Salter D, Elflick A: **Finite element simulations of tip-enhanced Raman and fluorescence Spectroscopy.** *J. Phys. Chem. B* 2006, **110**:6692.
- [147] Stratton JA: *Electromagnetic Theory.* McGraw-Hill Book Company, Inc. 1941.
- [148] Metiu H: **Surface enhanced spectroscopy.** *Progr. Surf. Sci.* 1984, **17**:153.
- [149] Palik E (Ed): *Handbook of Optical Constants of Solids.* Springer, Berlin 2000.
- [150] [Note that for the calculations that refer to the field at the tip apex, the field is calculated at 0.125 nm below the apex to avoid numerical artifacts due to finite grid size].
- [151] Jackson JD: *Classical Electrodynamics, Volume I, Chapter II.* John Wiley and Sons, New York, third edition 1999.
- [152] Raether H: *Surface Plasmons on Smooth and Rough Surfaces and on Gratings.* Springer-Verlag 1988.
- [153] Geshev PI, Klein S, Witting T, Dickmann K, Hietschold M: **Calculation of the electric-field enhancement at nanoparticles of arbitrary shape in close proximity to a metallic surface.** *Phys. Rev. B* 2004, **70**:075402.
- [154] Aravind PK, Nitzan A, Metiu H: **The interaction between electromagnetic resonances and its role in spectroscopic studies of molecules adsorbed on colloidal particles or metal spheres.** *Surf. Sci.* 1983, **110**:189.
- [155] Pettinger B, Domke K, Zhang D, Schuster R, Ertl G: **Direct monitoring of plasmon resonances in a tip-surface gap of varying width.** *Phys. Rev. B* 2007, **76**:113409.
- [156] Berndt R, Gimzewski JK, Johansson P: **Inelastic tunneling excitation of tip-induced plasmon modes on noble-metal surfaces.** *Phys. Rev. Lett.* 1991, **67**:4878.
- [157] Aizpurua J, Apell SP, Berndt R: **Role of tip shape in light emission from the scanning tunneling microscope.** *Phys. Rev. B* 2000, **62**:2065.
- [158] Demming AL, Festy F, Richards D: **Plasmon resonances on metal tips: Understanding tip-enhanced Raman scattering.** *J. Chem. Phys.* 2005, **122**:184716.
- [159] [Here $d = 0$ nm is defined as corresponding to a 20-30 % decrease in the shear-force amplitude.].
- [160] Lueck HB, Daniel DC, McHale JL: **Resonance Raman study of solvent effects on a series of triarylmethane dyes.** *J. Raman Spectrosc.* 1993, **24**:363.
- [161] Beversluis MR, Bouhelier A, Novotny L: **Continuum generation from single gold nanostructures through near-field mediated intraband transitions.** *Phys. Rev. B* 2003, **68**:115433.
- [162] Moskovits M: **Surface-enhanced spectroscopy.** *Rev. Mod. Opt.* 1985, **57**:783.
- [163] Haes AJ, Haynes CL, McFarland AD, Schatz GC, Van Duyne RP, Zou S: **Plasmonic materials for surface-enhanced sensing and spectroscopy.** *MRS Bulletin* 2005, **30**:368.
- [164] McFarland AD, Young MA, Dieringer JA, Van Duyne RP: **Wavelength-scanned surface-enhanced raman excitation spectroscopy.** *J. Phys. Chem. B* 2005, **109**:11279.
- [165] Aravind PK, Metiu H: **The effects of the interaction between resonances in the electromagnetic response of a sphere-plane structure: applications to surface enhanced spectroscopy.** *Surf. Sci.* 1983, **124**:506.
- [166] Fowles R: *Introduction to Modern Optics.* Holt, Rinehart &

Winston, 2nd edition 1975.

- [167] Neacsu CC, van Aken BB, Fiebig M, Raschke M: **Tip-enhanced near-field second-harmonic imaging of the ferroelectric domain structure of YMnO_3** . [To be published].
- [168] Lee KG, Kihm HW, Kihm JE, Choi WJ, Kim H, Ropers C, Park DJ, Yoon YC, Choi SB, Woo DH, Kim J, Lee B, Park QH, Lienau C, Kim DS: **Vector field microscopic imaging of light**. *Nat. Photon.* 2006, **1**:53.
- [169] Gersen H, Novotny L, Kuipers L, van Hulst NF: **On the concept of imaging nanoscale vector fields**. *Nat. Photon.* 2007, **1**:242.
- [170] Lee KG, Kihm HW, Kihm JE, Choi WJ, Kim H, Ropers C, Park DJ, Yoon YC, Choi SB, Woo DH, Kim J, Lee B, Park QH, Lienau C, Kim DS: **On the concept of imaging nanoscale vector fields**. *Nat. Photon.* 2007, **1**:243.
- [171] Poborchii V, Tada T, Kanayama T: **Subwavelength-resolution raman microscopy of Si structures using metal-particle-topped AFM probes**. *Jap. J. Appl. Phys.* 2005, **44**:202.
- [172] Schneider S, Brehm G, Freunschdt P: **Comparison of surface-enhanced Raman and hyper-Raman spectra of the triphenylmethane dyes crystal violet and malachite green**. *Phys. Stat. Sol. B* 1995, **189**:37.
- [173] Polubotko AM: **SERS phenomenon as a manifestation of quadrupole interaction of light with molecules**. *Phys. Lett.* 1990, **146**:81.
- [174] Sass JK, Neff H, Moskovits M, Holloway S: **Electric field gradient effects on the spectroscopy of adsorbed molecules**. *J. Phys. Chem* 1981, **85**:621.
- [175] Creighton J: *Spectroscopy of Surfaces*, John Wiley & Sons, New York, *Volume Vol 16 of Advances in Spectroscopy* 1988 chap. Selection Rules for Surface-enhanced Raman Spectroscopy, :37.
- [176] Ayars EJ, Hallen HD, Jahncke CL: **Electric field gradient effects in Raman spectroscopy**. *Phys. Rev. Lett.* 2000, **85**:4180.
- [177] Moskovits M: **Surface selection rules**. *J. Chem. Phys.* 1982, **77**:4408.
- [178] Erdheim GR, Birke RL, Lombardi JR: **Surface enhanced Raman spectrum of pyrazine. Observation of forbidden lines at the electrode surface**. *Chem. Phys. Lett.* 1980, **69**:495.
- [179] Dornhaus R, Long MB, Benner RE, Chang RK: **Time development of sers from pyridine, pyrimidine, pyrazine, and cyanide adsorbed on ag electrodes during an oxidation-reduction cycle**. *Surf. Sci.* 1980, **93**:240.
- [180] Moskovits M, Dilella DP: **Enhanced Raman spectra of ethylene and propylene adsorbed on silver**. *Chem. Phys. Lett.* 1980, **73**:500.
- [181] Maher RC, Cohen LF, Etchegoin P: **Single molecule photo-bleaching observed by surface enhanced resonant Raman scattering (SERRS)**. *Chem. Phys. Lett.* 2002, **352**:378.
- [182] Wang Z, Rothberg LJ: **Origins of blinking in single-molecule Raman spectroscopy**. *J. Phys. Chem.* 2005, **109**:3387.
- [183] Xie XS, Trautman JK: **Optical studies of single molecules at room temperatures**. *Annu. Rev. Phys. Chem.* 1998, **49**:441.
- [184] Moyer P, Smith J, Eng L, Meixner A: **Surface-Enhanced Raman scattering spectroscopy of single carbon domains on individual Ag nanoparticles on a 25 ms time scale**. *J. Am. Chem. Soc.* 2000, **122**:5409.
- [185] Kudelski A, Pettinger B: **SERS on carbon chain segments: monitoring locally surface chemistry**. *Chem. Phys. Lett* 2000, **321**:356.
- [186] Picardi G: **Raman spectroscopy and light emission at metal surfaces enhanced by the optical near-field of a scanning tunneling tips**. *PhD thesis*, Freie Universität Berlin 2003.
- [187] Futamata M, Maruyama Y, Ishikawa M: **Critical importance of the junction in touching Ag particles for single molecule sensitivity in SERS**. *J. Molec. Struct.* 2005, **735**:75.
- [188] Le Ru EC, Etchegoin PG, Meyer M: **Enhancement factor distribution around a single SERS Hot-spot and its relation to Single Molecule detection**. *J. Chem. Phys.* 2006, **125**:204701.
- [189] Friedrich B, Herschbach D: **Alignment and trapping of molecules in intense laser fields**. *Phys. Rev. Lett.* 1995, **74**:4623.
- [190] Chen JY, Wiley BJ, Xia YN: **One-dimensional nanostructures of metals: Large-scale synthesis and some potential applications**. *Langmuir* 2007, **23**:4120.
- [191] Zhu Y, Ke C, Espinosa HD: **Experimental techniques for the mechanical characterization of one-dimensional nanostructures**. *Exp. Mech.* 2007, **47**:7.
- [192] Wang ZL: **New developments in transmission electron microscopy on the nanoscale**. *Adv. Mat.* 2003, **15**:1497.
- [193] Zhang XF, Zhang Z: *Progress in Transmission Electron Microscopy 2: Applications in Materials Science (Springer Series in Surface Sciences)*. Springer 2001.
- [194] Zuo JM, Vartanyants I, Gao M, Zhang R, Nagahara LA: **Atomic resolution imaging of a carbon nanotube from diffraction intensities**. *Science* 2003, **300**:1419.
- [195] Chapman HN, Barty A, Marchesini S, Noy A, Hau-Riege SP, Cui C, Howells MR, Rosen R, He H, Spence JCH, Weierstall U, Beetz T, Jacobsen C, Shapiro D: **High-resolution ab initio three dimensional x-ray diffraction microscopy**. *J. Opt. Soc. Am. A* 2006, **5**:1179.
- [196] M DiDomenico SHW, Porto SPS: **Raman spectrum of single-domain BaTiO_3** . *Phys. Rev.* 1968, **174**:522–530.
- [197] Li Z, Foster CM, Dai XH, Xu XZ, Chan SK, Lam DJ: **Piezoelectrically-induced switching of 90 degree domains in tetragonal BaTiO_3 and PbTiO_3 investigated by micro-Raman spectroscopy**. *J. App. Phys.* 1992, **71**(9):4481–4486.
- [198] Nakamura M, Orihara H, Ishibashi Y, Hara K: **Observation of ferroelastic domains in LaNbO_4 by micro-Raman spectroscopy**. *J. Phys. Soc. Jap.* 1990, **59**:4472–4475.
- [199] Gardiner DJ: *Practical Raman Spectroscopy*. Springer Verlag 1989.
- [200] Drago RS: *Physical Methods for Chemists*. Surfside Scientific Publishers 1992.
- [201] C A Arguello DL, Porto SPS: **First-order raman effect in wurtzite-type crystals**. *Phys. Rev.* 1969, **181**:1351.
- [202] Lee N, Hartschuh RD, Mehtani D, Kisliuk A, Maguire JF, Green M, Foster MD, Sokolov AP: **High contrast scanning nano-Raman spectroscopy of silicon**. *J. Raman Spectrosc.* 2007, **38**:789–796.
- [203] Nguyen Q, Ossikovski R, Schreiberb J: **Contrast enhancement on crystalline silicon in polarized reflection mode tip-enhanced Raman spectroscopy**. *Science Direct* 2007, **274**:231–235.
- [204] Saito Y, Motohashi M, Hayazawa N, Iyoki M, S Kawata S: **Nanoscale characterization of strained silicon by tip-enhanced Raman spectroscopy in reflection mode**. *Appl. Phys. Lett.* 2006, **88**:143109.
- [205] Berweger S, Neacsu CC, Raschke MB: *manuscript in preparation*.
- [206] Mao Y, Banerjee S, Stanislaus S Wong SS: **Large-scale synthesis of single-crystalline perovskite nanostructures**. *J. Am. Chem. Soc.* 2003, **125**:15718.
- [207] Blinc R: **Order and disorder in perovskites and relaxor ferroelectrics**. *Structure Bond* 2007, **124**:51.
- [208] Gheno SM, Hasegawa HL, Filho PIP: **AFM characterization**

- of Barium Titanate.** *Ferroelec.* 2006, **334**:43.
- [209] Buscaglia MT, Viviani M, Buscaglia V, Mitoseriu L, Testino A, Nanni P, Zhao Z, Nygren M, Harnagea C, Piazza D, Galassi C: **High dielectric constant and frozen macroscopic polarization in dense nanocrystalline BaTiO₃ ceramics.** *Phys. Rev. B* 2006, **73**(6):064114.
- [210] Fan HM, Fan XF, Ni ZH, Shen ZX, Feng YP, Zou BS: **Orientation-dependent Raman spectroscopy of single wurtzite CdS nanowires.** *J. Phys. Chem. C* 2008, **112**:1865.
- [211] Moerland RJ, Taminiau TH, Novotny L, van Hulst NF, Kuipers L: **Reversible polarization control of single photon emission.** *Nano Lett.* 2008.
- [212] Ayars E, Jahncke C, Paesler M, Hallen H: **Fundamental differences between micro- and nano-Raman spectroscopy.** *J. Microsc.* 2001, **202**:142.
- [213] Ropers C, Neacsu CC, Elsaesser T, Albrecht M, Raschke MB, Lienau C: **Grating-coupling of surface plasmons onto metallic tips: A nanoconfined light source.** *Nano Lett.* 2007, **7**:2784. [Featured in: Nature Photonics 446, 500].
- [214] Stockman MI, Bergman DJ, Anceau C, Brasselet S, Zyss J: **Enhanced second-harmonic generation by metal surfaces with nanoscale roughness: Nanoscale dephasing, depolarization, and correlations.** *Phys. Rev. Lett.* 2004, **92**:057402.
- [215] Ebbesen TW, Lezec HJ, Ghaemi HF, Thio T, Wolff PA: **Extraordinary optical transmission through sub-wavelength hole arrays.** *Nature* 1998, **391**:667.